Energetic Couplings in Ferroics

Hong Jian Zhao, Peng Chen, Sergey Prosandeev, Charles Paillard, Kinnary Patel, Jorge Íñiguez, Laurent Bellaiche

Energetic couplings in ferroics

Hong Jian Zhao Peng Chen Sergey Prosandeev Charles Paillard Kinnary Patel Jorge Íñiguez Laurent Bellaiche*

Prof. Hong Jian Zhao
International Center for Computational Method and Software, College of Physics, Jilin University, Changchun 130012, China
Physics Department and Institute for Nanoscience and Engineering, University of Arkansas, Fayetteville, Arkansas 72701, USA
Email Address: physzhaohj@jlu.edu.cn (H.J.Z.)
Dr. Peng Chen, Prof. Sergey Prosandeev, Dr. Kinnary Patel, Prof. Laurent Bellaiche
Physics Department and Institute for Nanoscience and Engineering, University of Arkansas, Fayetteville, Arkansas 72701, USA
Prof. Charles Paillard
Laboratoire SPMS, CentraleSuplec/CNRS UMR8580, Université Paris-Saclay, 8-10 Rue Joliot-Curie, 91190 Gif-sur-Yvette, France
Prof. Jorge Íñiguez
Materials Research and Technology Department, Luxembourg Institute of Science and Technology (LIST), Avenue des Hauts-Fourneaux 5, L-4362 Esch/Alzette, Luxembourg
Physics and Materials Science Research Unit, University of Luxembourg, 41 Rue du Brill, L-4422 Belvaux, Luxembourg

Keywords: *Phenomenological theories, Ferroics, Perovskites*

Ferroics include diverse degrees of freedom (such as structural distortions and magnetic moments) among which cross couplings occur, rendering a large variety of interesting phenomena. Determining such couplings, based on symmetry analysis, is not only important to interpret observed phenomena but can also result in novel predictions to be then experimentally checked. Often, such energetic couplings are difficult to construct without a deep knowledge of group theoretical symmetry principles. In the present review, a crash course towards the derivation of energetic couplings, without using much the group theoretical language, is provided. Rather, the present approach relies on a graphical technique and suitable symbolic language, which naturally yields some known couplings (resulting in, e.g., spin/dipole canting, magnetically driven polarization and antipolar/antiferroelectric states). This review also reports and discusses other symmetry-allowed energetic terms, including some leading to the occurrence of an electric polarization in a variety of materials, and "exotic" ones that generate complex phases and phenomena in, e.g., nanostructures and heterostructures.

1 Introduction

Ferroelectric, ferroelastic, magnetic and multiferroic materials – namely, ferroic materials – play a crucial role in many fields such as information storage and sensing[1–3]. Besides, there are various degrees of freedom, such as structural distortions and magnetic moments, that are often crossly coupled and that are at the heart of intriguing phenomena. Examples includes improper ferroelectricity[4–8], spin canting[9–11], magnetic compensation temperatures[11,12], and a variety of magnetoelectric effects[13–15]. Some excellent reviews have already been written regarding the advancement of ferroic materials (in particular, multiferroics) in the fields of theory, experiment and application, see, e.g., Refs.[16–21]. On the other hand, it appears that a review article solely devoted to the fundamental energetic couplings responsible for these ferroic and multi-ferroic effects is currently missing, to the best of our knowledge.

For instance, we have previously proposed a variety of symmetry-allowed energetic couplings (mostly, focusing on $AB\mathrm{O}_3$ perovskites), including those involving anti-polar motions of A cations induced by oxygen octahedral tiltings[22–24], hybrid improper ferroelectricity in $AB\mathrm{O}_3/A'B\mathrm{O}_3$ superlattices[8], electrical polarization resulting from the simultaneous occurrence of two magnetic sublattices[25,26], spin canting arising from magnetic Dzyaloshinskii–Moriya interactions (DMI) induced by oxygen octahedral tiltings[9,12] and its corresponding effects for canted electric dipoles in ferroelectric and antiferroelectrics[26], as well as high-order magnetoelectric couplings[13,14]. Here, we shall revisit these energetic couplings not by simply re-introducing them one by one, but rather by re-deriving some of them in an original and straightforward

fashion. Note that such energetic couplings not only can explain some experimentally-observed phenomena, but also can be put in use to predict novel effects. We also provide two additional sections: one describing various ways to induce electrical polarization in different types of materials, and one discussing even more "exotic" energetic terms that have been proposed to give rise to, or simply explain, some striking phenomena in ferroics.

2 Deriving symmetry-allowed energetic couplings

Let us first take ABX_3 perovskites (with X typically being O, F, Cl or I ions) as our platform, since these materials are known to host diverse degrees of freedom – say, order parameters related to structural distortions and/or magnetic orders. Note, however, that our approaches, to be explained below, can be easily generalized to non-perovskite systems. In the present review, the basic spirit is to form energetic couplings involving various order parameters, with these energetic terms being invariant under *all* symmetry operations of the high-symmetric reference phase of the considered system.

2.1 Definition of the order parameters

2.1.1 Displacements, rotations and magnetic moments

The ideal ABX_3 perovskite is cubic with a $Pm\bar{3}m$ space group[27]. When structural distortions occur, the symmetry deviates from $Pm\bar{3}m$. By structural distortions, here we mean collective atomic displacements involving the A, B, and/or X ions. Let us first define the physical quantities that can be associated to each ion. In **Figure 1(b)**, one chosen ion is originally located at the "a" position (dashed circle) and then located at the "a′" position (solid circle) after being displaced by $\mathbf{u}$ (red arrow). We can thus identify a quantity (i.e., the atomic displacement $\mathbf{u}$) which is invariant under time-reversal operation ($1'$). Indeed, time-reversal transforms the time t to $-t$ but has no effects on spatial coordinates (see Figure 1(a)). On the other hand, as shown in Figure 1(c), the displacement $\mathbf{u}$ is transformed to $-\mathbf{u}$ by spatial inversion ($\bar{1}$).

Now, we turn to the rotation of the BX_6 octahedron shown in Figure 1(e), where the green and yellow spheres denote the B and X ions, respectively. The yellow sphere with the number i corresponds to the X_i ion, and the red arrows originating from X_3, X_4, X_5 and X_6 ions denote the displacements associated to them. In Figure 1(e), the rotation allows us to define a $\boldsymbol{\omega}$ pseudo-vector located on the B ion and pointing towards X_1, based on the right-hand rule. For instance, $\boldsymbol{\omega} = 0.1\hat{z}$, where $\hat{z}$ is the unit vector along the z-axis, corresponds to a tilting of about 0.1 radians of the BX_6 octahedron about such z-axis. We graphically denote such $\boldsymbol{\omega}$ pseudo-vector by the bold green arrow (lower left corner of Figure 1(e)). The time-reversal transformation has no effect on $\boldsymbol{\omega}$. Indeed, both the positions of the X_i ions and their associated displacements are invariant under time-reversal (see Figure 1(d)). Moreover, under a spatial inversion centered in the B cation, the X ions swaps their positions by pairs (X_3 swaps with X_4, X_5 with X_6, and X_1 with X_2), and the corresponding displacement vectors reverse signs as well (see Figure 1(f)). As a result, the $\boldsymbol{\omega}$ pseudo-vector is invariant under inversion.

Furthermore, some A or B ions (*e.g.*, Gd^{3+} and Fe^{3+} in $GdFeO_3$) can carry magnetic moments as well. In order to discuss the symmetry properties of magnetic moments, it is convenient to imagine the magnetic moment as originating from an electric current loop, following classical electromagnetism. (Strictly speaking, this picture is appropriate only if we are dealing with orbital magnetism; yet, symmetry-wise, it works for the magnetic moments associated to electronic spins as well.) For example, by the right-hand rule, the electric current (flowing from "b" to "c", in Figure 1(h)) results in a magnetic moment $\mathbf{m}$ pointing upwards (blue arrow). Notice that the electric current $I = \frac{dQ}{dt}$ (Q is the electric charge) depends on the sign of time. Under time reversal, the electric current now flows from "c" to "b" and the magnetic moment is transformed to $-\mathbf{m}$ (see Figure 1(g)). On the other hand, if we apply a spatial inversion transformation, electric current from "b" and "c" becomes a current from "b′" to "c′"; hence the magnetic moment is invariant under inversion (*cf* Figure 1(i)).

To summarize this part, the displacement vector $\mathbf{u}$ is invariant under time reversal but reverses its sign under spatial inversion; the magnetic moment $\mathbf{m}$ transforms in just the opposite way from $\mathbf{u}$. Ionic

displacements can also happen in a collective way, which, e.g., leads to a pseudo-vector $\boldsymbol{\omega}$, that is invariant under both inversion and time reversal. Henceforth, we shall construct order parameters for perovskites using such $\mathbf{u}$, $\mathbf{m}$, and $\boldsymbol{\omega}$ building blocks.

2.1.2 Order parameters

We now focus on order parameters associated with structural distortions and magnetic structures in ABX_3 perovskites.

Common distortions are the anti-phase and in-phase tiltings of the BX_6 octahedra (Figure 2). As explained in Section 2.1.1., notice should be taken that (i) the anti-phase and in-phase tiltings essentially are displacements carried by the X ions, but (ii) such displacements can be characterized by $\boldsymbol{\omega}$ pseudo-vectors centered at the B ions (Figs. 1(d)-(f)). Taking the case of the $\boldsymbol{\omega}$'s being oriented along the z [001] pseudocubic axis as an example, the ionic motions involved in anti-phase tiltings are shown in Figure 2(a) and represented by $\boldsymbol{\omega}$ vectors in a way demonstrated in Figure 2(b). Similarly, we show and represent the case of in-phase tiltings about the $z-$axis in Figs. 2(c) and (d), respectively.

Let us now mathematically represent these structural distortions. To this end, we introduce the definition of $q-$points and its modulations in Figure 3. Such definitions can be found in Ref.[28] (see *e.g.*, its Supplementary Information) and we repeat it here for sake of the completeness and understanding. The $Pm\bar{3}m$ cubic perovskite has a 5-atom primitive cell whose lattice vectors are denoted as $\mathbf{a}_x$, $\mathbf{a}_y$, and $\mathbf{a}_z$ (note that these three latter vectors are along the [100], [010] and [001] pseudo-cubic directions, respectively). Selecting an arbitrary direct lattice site as the origin point, the rest of the direct lattice sites (which can be each associated with a specific 5-atom cell) are represented by a lattice vector $l_x\mathbf{a}_x+l_y\mathbf{a}_y+l_z\mathbf{a}_z \equiv (l_x, l_y, l_z)$, where l_x, l_y, and l_z are integers. Similarly, we define the reciprocal lattice vectors $\mathbf{a}_x^\star$, $\mathbf{a}_y^\star$, and $\mathbf{a}_z^\star$; then, the $q-$points belonging to the first Brillouin zone of the cubic perovskite structure can be indexed as $\mathbf{q} = q_x\mathbf{a}_x^\star + q_y\mathbf{a}_y^\star + q_z\mathbf{a}_z^\star \equiv (q_x, q_y, q_z)$. Notice that q_α ($\alpha = x, y, z$) are non integers and $\mathbf{a}_\alpha \cdot \mathbf{a}_\beta^\star = 2\pi\delta_{\alpha,\beta}$. In particular, the eight $q-$points indicated in Figure 3(b) are classified into four categories: (i) the Γ point which corresponds to homogeneous repetitions of our local quantities (*e.g.*, an homogeneous repetition of the local $\mathbf{u}$-vectors leads to a ferroelectric distortion) that are thus invariant for any arbitrary lattice translation, (ii) the R point that involves an anti-phase spatial modulation of the local quantities (*e.g.*, the $\boldsymbol{\omega}$ pseudo-vectors), thus reversing sign when translating by one lattice vector along the x, y or z direction, (iii) the $M\alpha$ point that involves a different type of modulation, whereby the local quantities (*e.g.*, the magnetic moments) are invariant upon lattice translations along the α-axis but reverse their sign upon lattice translations perpendicular to the α-axis, and (iv) the $X\alpha$ point that involves yet another type of modulation whereby the local quantities are invariant upon lattice translations perpendicular to the α-axis while they reverse their sign upon translations parallel to the α-axis.

Let us take the anti-phase and in-phase tiltings as examples to demonstrate how to link the physical local quantities to a specific $q-$point. The basic idea is to form *collective* modes spanning the whole lattice coordinate space containing N primitive cells. For anti-phase tiltings, any two nearest-neighboring BX_6 octahedra rotate in anti-phase to each other. We can thus express the $\boldsymbol{\omega}$ pseudo-vector associated to the (l_x, l_y, l_z) lattice site as

$$\boldsymbol{\omega}(l_x, l_y, l_z) = (-1)^{(l_x+l_y+l_z)}\boldsymbol{\omega} \equiv e^{-2\pi i(q_x l_x+q_y l_y+q_z l_z)}\boldsymbol{\omega} \tag{1}$$

where, for anti-phase tiltings, $(q_x, q_y, q_z) = (\frac{1}{2}, \frac{1}{2}, \frac{1}{2})$ is identified as the R point by comparing Figure 2(b) and Figure 3(b). We thus represent anti-phase tiltings about the z-axis (Figure 2(b)) in terms of an order parameter defined as:

$$\omega_z^R = \frac{1}{N}\sum_{l_x,l_y,l_z} e^{2\pi i(q_x l_x+q_y l_y+q_z l_z)}\omega_z(l_x, l_y, l_z) \tag{2}$$

where the superscript R and subscript z mark the corresponding q point and orientation of the collective mode ω_z^R, respectively. Similarly, one can describe the in-phase tilting about the $z-$axis as:

$$\omega_z^{Mz} = \frac{1}{N}\sum_{l_x,l_y,l_z} e^{2\pi i(q_x l_x + q_y l_y + q_z l_z)}\omega_z(l_x,l_y,l_z) \quad (3)$$

where now we have $(k_x,k_y,k_z) = (\frac{1}{2},\frac{1}{2},0)$, which is identified as the Mz q-point (see Figure 3b). Similarly, in-phase tiltings about the $x-$ or $y-$axis involve the Mx and My q-point, respectively. So far, we have thus arrived at the symbolic representation of anti-phase and in-phase BX_6 tiltings (termed as tilting order parameters), via $\omega_\alpha^q = \frac{1}{N}\sum_{l_x,l_y,l_z} e^{2\pi i(q_x l_x + q_y l_y + q_z l_z)}\omega_\alpha(l_x,l_y,l_z)$ with $q = (\frac{1}{2},\frac{1}{2},\frac{1}{2})$, $(\frac{1}{2},\frac{1}{2},0)$, $(\frac{1}{2},0,\frac{1}{2})$, and $(0,\frac{1}{2},\frac{1}{2})$ that are, respectively, associated with R, Mz, My and Mx points (see also Figure 3(b)).

In ABX_3 perovskites, the displacement $\mathbf{u}$ and magnetic moment $\mathbf{m}$ vectors can be associated to B and/or A ions. For example, in Figure 3(c), the A or B sublattice is magnetized with the blue arrow denoting the magnetic moment $\mathbf{m}$. In such a case, with the $\mathbf{m}$ vectors pointing along the $\pm x$ direction, the magnetic moments within the yz plane are ferromagnetically coupled to each other while they are antiferromagnetically coupled to each other between two sites separated by $\pm\mathbf{a}_x$. This magnetic structure is accordingly denoted by the symbol m_x^{Xx}, since the local magnetic moments $\mathbf{m}$ point along the $\pm x$ direction and are modulated according to the Xx point (defined in Figure 3(b) and for which the corresponding $q-$point is $(\frac{1}{2},0,0)$). Note that the close relatives of Xx point are the Xy and Xz points whose reciprocal coordinates are $(0,\frac{1}{2},0)$ and $(0,0,\frac{1}{2})$, respectively. Moreover, Figure 3(d) displays a displacement $\mathbf{u}$ associated to either the A or B sublattice, along the z direction and modulated according to the My q-point. This displacement collective mode is thus denoted by u_z^{My}.

So far, in this subsection we have defined eight important $q-$points, and shown how to represent some order parameters symbolically. Specifically, order parameters, linked to the α-component of any local physical vectors $\mathbf{r}$ (*e.g.,* $\mathbf{r}$ can be the displacements $\mathbf{u}$, pseudo-vectors $\boldsymbol{\omega}$, and magnetic moments $\mathbf{m}$) and being modulated according to a $q-$point can be generally expressed as

$$r_\alpha^q = \frac{1}{N}\sum_{l_x,l_y,l_z} e^{2\pi i(l_x q_x + l_y q_y + l_z q_z)} r_\alpha(l_x,l_y,l_z) \quad (4)$$

Thanks to these notations, we are now ready to enumerate the typical order parameters in ABX_3 perovskites, which are summarized in Table 1. Note that the displacement $\mathbf{u}$ and magnetic moments $\mathbf{m}$ can be associated to both A and B sublattices, and these two cases must be distinguished. Hence, to further define displacement or magnetic order parameters, we use the notation $r_{Y,\alpha}^q$ ($\mathbf{r} = \mathbf{u}$ or $\mathbf{r} = \mathbf{m}$), where $Y = A, B$ denote the atomic sublattice to which the physical quantity is associated. On the other hand, the rotation-related pseudo-vector $\boldsymbol{\omega}$ can only be centered in the B sublattice in perovskites, and we thus simply use ω_α^q to denote it. Finally, let us indicate that the homogeneous strain order parameters $\eta_{\alpha\beta}$ (α and β being x, y, and z) can also be defined; further, they are associated to the Γ point and affect the full lattice (i.e., they affect all A, B, or X atomic sublattices). Let us also emphasize that $\eta_{\alpha\beta}$ transforms under symmetry operations exactly as the product $u_{Y,\alpha}^\Gamma u_{Y,\beta}^\Gamma$.

2.2 Transformation of the order parameters

Before (re)deriving some energetic couplings, there is one last obstacle to overcome: we should know the symmetry operations of the considered systems and the transformations of each of the order parameter under such operations. Since our order parameters in Table 1 are defined with respect to the cubic $Pm\bar{3}m$ perovskite structure, the energetic couplings have to be invariant under the symmetry operations of the $Pm\bar{3}m$ space group. There are plenty of symmetry operations for this space group, including the infinite number of lattice translation operations, forty-eight point operations and time-reversal symmetry. Fortunately, all these crystallographic symmetry operations are simply generated by a small subset of them: (i) the two-fold rotation about the [001] direction (2_{001}), the two-fold rotation about the [010] direction (2_{010}), the three-fold rotation about the [111] direction (3^+_{111}), the two-fold rotation about the [110] direction (2_{110}), and the inversion ($\bar{1}$); (ii) time-reversal ($1'$); and (iii) the lattice translations given

by the $\mathbf{a}_x$, $\mathbf{a}_y$, and $\mathbf{a}_z$ vectors, in the following denoted by $T(\mathbf{a}_x)$, $T(\mathbf{a}_y)$, and $T(\mathbf{a}_z)$, respectively. These operations are termed as "generators" of the space group, and can be found at `https://www.cryst.ehu.es/cryst/get_gen.html`. Notice again that the [100], [010], and [001] directions coincide with our x, y, and z pseudo-cubic axes, respectively.

Let us now demonstrate how various order parameters transform under the point and time-reversal symmetry operations, as schematized in Figure 4. We first take the order parameter $u^{Xx}_{B,z}$ as an example, recalling that it represents the collective displacements (along the z direction) carried by the B ionic sublattice and modulated according to the Xx reciprocal-space point. The original order parameter (*i.e.*, before transformation) is shown in Figure 4(a) with eight B ions labelled by i (*i.e.*, B_i with $i = 1, ..., 8$). The 2_{110} operation transforms the situation in Figure 4(a) into the situation in Figure 4(b), and three changes have occurred *simultaneously*: (i) the ions B_1, B_2, B_3, and B_4 are interchanged with B_5, B_8, B_7, and B_6, respectively; (ii) the displacements originally along the $+z$ direction (associated to the B_1, B_4, B_5, and B_8 ions) now point along $-z$; (iii) conversely, the displacements originally along the $-z$ direction (associated to the B_2, B_3, B_6, and B_7 ions) now point along the $+z$ direction. Translating the sketches into symbolic language, we see the transformation from $u^{Xx}_{B,z}$ to $-u^{Xy}_{B,z}$ under the 2_{110} operation, noticing, in particular, that the 2_{110} rotation changes the $q-$point (*i.e.*, the spatial modulation) from Xx to Xy.

Similarly, comparing Figure 1(d) and Figure 1(e), $m^{Xx}_{B,z}$ is transformed to $-m^{Xy}_{B,z}$ by 2_{110}. Indeed, the order parameter $r^q_{Y,\alpha}$ always transforms identically by proper rotation operations (*i.e.*, rotations without combining with $\bar{1}$ or $1'$), regardless of whether $\mathbf{r}$ is $\mathbf{u}$, $\mathbf{m}$, or $\boldsymbol{\omega}$[29]. Comparing Figs. 4(a) and 4(c), the inversion leaves $u^{Xx}_{B,z}$ invariant. On the other hand, the inversion transforms $m^{Xx}_{B,z}$ into $-m^{Xx}_{B,z}$, because the inversion transforms $\mathbf{m}$ and $\mathbf{u}$ in different way (see Section **2.1.1**). Note also that, in general, the proper rotation symmetry operations, denoted by n_α (e.g., $n-$fold rotation axis about the α-axis), can be combined with inversion to form the so-called improper rotations[29]. For example, the combination of 2_{001} with $\bar{1}$ is equivalent to the mirror plane perpendicular to the [001] orientation. If we need to transform an order parameter by a improper rotation, we thus "just" need to transform it by the proper rotation n_α followed by an additional inversion transformation. Finally, the time-reversal operation has no effect on $u^q_{Y,\alpha}$ and ω^q_α, but always transforms $m^q_{Y,\alpha}$ to $-m^q_{Y,\alpha}$. Using the graphical rule depicted in Figure 4, the transformations of the various order parameters under point operations and time-reversal symmetry are readily obtained and summarized in Table 1.

Regarding the transformation of the order parameters under the $T(\mathbf{a}_\beta)$ translations, it depends on their $q-$point modulations. For instance, let us consider the transformation of $r^q_{Y,\alpha} = \frac{1}{N}\sum_{l_x,l_y,l_z} e^{2\pi i(q_x l_x + q_y l_y + q_z l_z)}$ $r_{Y,\alpha}(l_x, l_y, l_z)$ under, e.g., $T(\mathbf{a}_x)$. Since $T(\mathbf{a}_x)$ changes $r_{Y,\alpha}(l_x, l_y, l_z)$ to $r_{Y,\alpha}(l_x - 1, l_y, l_z)$, we have

$$r^q_{Y,\alpha} \rightarrow \frac{1}{N}\sum_{l_x,l_y,l_z} e^{2\pi i(q_x l_x + q_y l_y + q_z l_z)} r_{Y,\alpha}(l_x - 1, l_y, l_z)$$

$$= e^{2\pi i q_x}\frac{1}{N}\sum_{l_x,l_y,l_z} e^{2\pi i(q_x l_x + q_y l_y + q_z l_z)} r_{Y,\alpha}(l_x, l_y, l_z) = e^{2\pi i q_x} r^q_{Y,\alpha}\ . \tag{5}$$

More generally, $T(\mathbf{a}_\kappa)$ transforms $r^q_{Y,\alpha}$ into $e^{2\pi i q_\kappa} r^q_{Y,\alpha}$, where κ is the direction, *e.g.*, x, y, or z.

In summary, we emphasize that $u^q_{Y,\alpha}$, $m^q_{Y,\alpha}$, and ω^q_α are three types of order parameters that are key to understand the physical properties of many perovskites. In this section we have seen that (i) under the pure proper rotations, $u^q_{Y,\alpha}$ and $m^q_{Y,\alpha}$ (as well as $u^q_{B,\alpha}$, $m^q_{B,\alpha}$ and ω^q_α) transform identically; (ii) under time-reversal, $u^q_{Y,\alpha}$ and ω^q_α remain invariant, while $m^q_{Y,\alpha}$ becomes $-m^q_{Y,\alpha}$; and (iii) under improper rotations (inversion center, mirror planes), $m^q_{B,\alpha}$ and ω^q_α transform identically, but in an opposite way than $u^q_{B,\alpha}$.

2.3 Principles for energetic couplings

Now we are ready to construct the energetic couplings making use of Table 1. Notice that we still limit ourselves to perovskites at this moment. Readers might realize that we can easily guess a term, like, e.g., a bilinear coupling UV (U, V being two order parameters), and prove that such a term (to be discussed

later) is invariant under (i) the translations $T(\mathbf{a}_x)$, $T(\mathbf{a}_y)$, $T(\mathbf{a}_z)$; (ii) the rotations 2_{001}, 2_{010}, 3_{111}, 2_{110}, $\bar{1}$; and (i) the time-reversal ($1'$). Indeed, this is exactly the basic principle, i.e., the energetic coupling must be invariant under *all* the generators of the reference phase (e.g., the $Pm\bar{3}m$ space group plus time-reversal symmetry in perovskites). In the following, we will arrive at some rules that can simplify our analysis when constructing energetic couplings.

2.3.1 Rules from translation symmetry

Given two order parameters $r^{\mathbf{q_1}}_{Y_1,\alpha}$ and $r^{\mathbf{q_2}}_{Y_2,\beta}$ (Y_1 and Y_2 being A or B), a coupling $r^{\mathbf{q_1}}_{Y_1,\alpha}r^{\mathbf{q_2}}_{Y_2,\beta}$ is readily formed. Under $T(\mathbf{a}_\kappa)$, we have the transformation $r^{\mathbf{q_1}}_{Y_1}r^{\mathbf{q_2}}_{Y_2,\beta} \rightarrow e^{2\pi i(q_{1\kappa}+q_{2\kappa})}r^{\mathbf{q_1}}_{Y_1}r^{\mathbf{q_2}}_{Y_2,\beta}$ following Eq. (5). To make $r^{\mathbf{q_1}}_{Y_1}r^{\mathbf{q_2}}_{Y_2,\beta}$ invariant under $T(\mathbf{a}_\kappa)$ (κ being x, y, or z), $e^{2\pi i(q_{1\kappa}+q_{2\kappa})}$ must be 1, so that $q_{1\kappa}+q_{2\kappa}$ must thus be an integer. In other words, given two order parameters modulated according to $\mathbf{q_1} = q_{1x}\mathbf{a}^\star_x + q_{1y}\mathbf{a}^\star_y + q_{1z}\mathbf{a}^\star_z \equiv (q_{1x}, q_{1y}, q_{1z})$ and $\mathbf{q_2} = q_{2x}\mathbf{a}^\star_x + q_{2y}\mathbf{a}^\star_y + q_{2z}\mathbf{a}^\star_z \equiv (q_{2x}, q_{2y}, q_{2z})$, their multiplication might be an energy invariant only if $\mathbf{q_1} + \mathbf{q_2} = \mathbf{G}$ with $\mathbf{G}$ a reciprocal lattice vector. If this condition is not satisfied, the translation symmetry will be violated. Similarly, for a potential invariant coupling n order parameters $r^{q_i}_{Y_i,\alpha_i}$ (i = 1 to n), translation symmetry requires $\sum_i q_{i\kappa}$ being integer for all κ, *i.e.*, $\sum_i \mathbf{q}_i = \mathbf{G}$.

2.3.2 Rules from time-reversal

For couplings involving magnetic order parameters (*e.g.*, $m^{\mathbf{q_i}}_{Y_i,\alpha}$), we have to consider time-reversal symmetry ($1'$) as well. Under this operation, we have the transformations $m^{\mathbf{q_i}}_{Y_i,\alpha} \rightarrow -m^{\mathbf{q_i}}_{Y_i,\alpha}$, $u^{\mathbf{q_i}}_{Y_i,\alpha} \rightarrow u^{\mathbf{q_i}}_{Y_i,\alpha}$, and $\omega^{\mathbf{q_i}}_{\alpha} \rightarrow \omega^{\mathbf{q_i}}_{\alpha}$. Hence, the coupling $\Pi_i r^{\mathbf{q_i}}_{Y_i,\alpha_i}$ may be invariant only if we have an even number of magnetic order parameters $m^{q_i}_{Y_i,\alpha}$ appearing in the product.

2.3.3 Constraints from rotation symmetry

We have many possible rotation operations. Here we present some examples to indicate how to deal with them. By now, we know that neither $m^R_{B,x}m^{Mx}_{A,y}$ nor $m^R_{B,x}\omega^R_x$ are energy invariants because the former violates translation symmetry while the later breaks the time-reversal operation. Then, one may wonder if, for instance, the coupling $m^R_{B,x}m^R_{B,y}$ is an invariant. To answer this question, we must consider the constraints from the rotation symmetry operations. Regarding $m^R_{B,x}m^R_{B,y}$, let us examine how this product is transformed by 2_{001}, 2_{010}, 3^+_{111}, 2_{110}, and $\bar{1}$. According to Table 1, we have, $m^R_{B,x}m^R_{B,y} \rightarrow m^R_{B,x}m^R_{B,y}$ under 2_{001}, $m^R_{B,x}m^R_{B,y} \rightarrow -m^R_{B,x}m^R_{B,y}$ by 2_{010}, $m^R_{B,x}m^R_{B,y} \rightarrow m^R_{B,y}m^R_{B,z}$ when applying 3^+_{111}, $m^R_{B,x}m^R_{B,y} \rightarrow m^R_{B,y}m^R_{B,x}$ under 2_{110}, and $m^R_{B,x}m^R_{B,y} \rightarrow m^R_{B,x}m^R_{B,y}$ by $\bar{1}$, respectively. We thus know that $m^R_{B,x}m^R_{B,y}$ is not an invariant because 2_{010} changes its sign.

What about the coupling $m^R_{B,x}m^R_{B,x}$? Here, we have $m^R_{B,x}m^R_{B,x} \rightarrow m^R_{B,x}m^R_{B,x}$ under 2_{100}, $m^R_{B,x}m^R_{B,x} \rightarrow m^R_{B,x}m^R_{B,x}$ by 2_{010}, $m^R_{B,x}m^R_{B,x} \rightarrow m^R_{B,y}m^R_{B,y}$ when applying 3^+_{111}, $m^R_{B,x}m^R_{B,x} \rightarrow m^R_{B,y}m^R_{B,y}$ by 2_{110}, and $m^R_{B,x}m^R_{B,x} \rightarrow m^R_{B,x}m^R_{B,x}$ under $\bar{1}$, respectively. $m^R_{B,x}m^R_{B,x}$ is thus not an invariant either because 3^+_{111} and 2_{110} change it to a different term, namely $m^R_{B,y}m^R_{B,y}$. Interestingly, this suggests that we can consider the coupling $m^R_{B,x}m^R_{B,x} + m^R_{B,y}m^R_{B,y} + m^R_{B,z}m^R_{B,z}$, which is indeed invariant and a legit (bilinear) energy coupling.

To end this subsection, we emphasize that to obtain an invariant energetic coupling term, we shall (i) first verify that the considered term that fulfills the rules from the translation symmetry (see Section **2.3.1**) and time-reversal (*cf* Section **2.3.2**), and (ii) then verify that it is also invariant under rotation symmetry operations.

2.3.4 Trilinear energetic term: an example

Let us now try to derive some trilinear energetic couplings. Before proceeding, we stress that there are many possibilities for trilinear energetic couplings involving the order parameters defined in Table 1. As an example, we consider here a trilinear term UVW with U and V being ω^R_α and $m^R_{B,\beta}$, respectively. Now the question is: what can the third order parameter W be? First, we quickly notice that the $q-$points for

ω_α^R and $m_{B,\beta}^R$ are both $(\frac{1}{2},\frac{1}{2},\frac{1}{2})$. If the $q-$point for the W order parameter is (q_x,q_y,q_z), the translation symmetry requires that $q_x+\frac{1}{2}+\frac{1}{2}$, $q_y+\frac{1}{2}+\frac{1}{2}$, and $q_z+\frac{1}{2}+\frac{1}{2}$ should all be integers; in other words, we must have$(q_x,q_y,q_z)\equiv\mathbf{G}$. Notice that the reciprocal $\mathbf{G}$ vector is equivalent to the Γ point since $e^{2\pi i(G_x l_x+G_y l_y+G_z l_z)}=1\equiv e^{2\pi i(0l_x+0l_y+0l_z)}$ always holds for l_x, l_y, and l_z integers. Hence, we conclude that W should be a Γ-point (homogeneous) order. On the other hand, invariance under time-reversal symmetry operation implies that W must be a magnetic order parameter. Thus, there are only two options for W, i.e., $m_{B,\gamma}^\Gamma$ or $m_{A,\gamma}^\Gamma$. Hence, we have that the possible energetic couplings might be $\omega_\alpha^R m_{B,\beta}^R m_{B,\gamma}^\Gamma$ or $\omega_\alpha^R m_{B,\beta}^R m_{A,\gamma}^\Gamma$.

However, this is not the end because we must confirm that $\omega_\alpha^R m_{B,\beta}^R m_{B,\gamma}^\Gamma$ or $\omega_\alpha^R m_{B,\beta}^R m_{A,\gamma}^\Gamma$ are invariant under rotation symmetry operations, and link α, β, and γ with the x, y, or z directions. We focus on $\omega_\alpha^R m_{B,\beta}^R m_{B,\gamma}^\Gamma$ and try four cases, e.g., $\alpha=\beta=\gamma$, $\alpha=\beta\neq\gamma$, $\alpha\neq\beta=\gamma$, and $\alpha\neq\beta\neq\gamma$, since such four cases exhaust all the possibilities. The $\alpha=\beta=\gamma$, $\alpha=\beta\neq\gamma$ and $\alpha\neq\beta=\gamma$ cases can be eliminated because under 2_{001}, $\omega_x^R m_{B,x}^R m_{B,x}^\Gamma \rightarrow -\omega_x^R m_{B,x}^R m_{B,x}^\Gamma$, $\omega_x^R m_{B,y}^R m_{B,y}^\Gamma \rightarrow -\omega_x^R m_{B,y}^R m_{B,y}^\Gamma$ and $\omega_x^R m_{B,x}^R m_{B,y}^\Gamma \rightarrow -\omega_x^R m_{B,x}^R m_{B,y}^\Gamma$. The reader may also want to verify that couplings such as $\omega_y^R m_{B,y}^R m_{B,y}^\Gamma$, $\omega_y^R m_{B,z}^R m_{B,z}^\Gamma$ and $\omega_y^R m_{B,y}^R m_{B,z}^\Gamma$ are not invariant under some rotation symmetry operations. Hence, our only hope to have an invariant of the form $\omega_\alpha^R m_{B,\beta}^R m_{B,\gamma}^\Gamma$ is the case with $\alpha\neq\beta\neq\gamma$ (e.g., $\omega_x^R m_{B,y}^R m_{B,z}^\Gamma$). Indeed, the 2_{001}, 2_{010}, and $\bar{1}$ symmetry operations all leave $\omega_x^R m_{B,y}^R m_{B,z}^\Gamma$ invariant. We now need a "closed" form based on $\omega_x^R m_{B,y}^R m_{B,z}^\Gamma$, which can be obtained by employing the 3_{111}^+ and 2_{110} operations. Considering (i) that 2_{110} transforms $\omega_x^R m_{B,y}^R m_{B,z}^\Gamma$ into $-\omega_y^R m_{B,x}^R m_{B,z}^\Gamma$, implying that $\omega_x^R m_{B,y}^R m_{B,z}^\Gamma-\omega_y^R m_{B,x}^R m_{B,z}^\Gamma$ is invariant under such operation, and (ii) the effect of 3_{111}^+ on these two terms, we can conclude that $\omega_x^R m_{B,y}^R m_{B,z}^\Gamma+\omega_y^R m_{B,z}^R m_{B,x}^\Gamma+\omega_z^R m_{B,x}^R m_{B,y}^\Gamma-\omega_y^R m_{B,x}^R m_{B,z}^\Gamma-\omega_z^R m_{B,y}^R m_{B,x}^\Gamma-\omega_x^R m_{B,z}^R m_{B,x}^\Gamma$ is invariant under the symmetry operations considered so far. In fact, we can easily confirm that such term, that can be rewritten in a compact way as $\boldsymbol{\omega}^R\cdot(\mathbf{m}_B^R\times\mathbf{m}_B^\Gamma)$, is invariant under *all* the generators of the $Pm\bar{3}m$ perovskite. Realizing that the order parameters $m_{B,\alpha}^\Gamma$ and $m_{A,\alpha}^\Gamma$ transform identically (see Table 1), another symmetry-allowed energetic term, namely $\boldsymbol{\omega}^R\cdot(\mathbf{m}_B^R\times\mathbf{m}_A^\Gamma)$, is thus obtained. In fact, the energetic terms $\boldsymbol{\omega}^R\cdot(\mathbf{m}_B^R\times\mathbf{m}_B^\Gamma)$ and $\boldsymbol{\omega}^R\cdot(\mathbf{m}_B^R\times\mathbf{m}_A^\Gamma)$ have already been used in phenomenological theories to interpret spin cantings in magnetic perovskites such as rare-earth orthoferrites and orthochromites[9,12,28,30,31]; we will be back to this in Section **3.3**.

2.3.5 Construction of energetic terms for materials beyond perovskites

To construct energetic couplings for non-perovskite materials, the procedures and basic principles are essentially identical to what is discussed above. We "only" need to pay attention to two specific aspects. First of all, for non-perovskite materials, we have to define new order parameters instead of the ones indicated in Table 1. Let us for instance assume that the phase of the target material, to be denoted as P_{low}, is of low symmetry. We thus have to find its corresponding high-symmetry reference phase P_{high} and define the order parameters of P_{low} with respect to P_{high}. Fortunately, some online softwares can help us do this. We will not show how to use these tools here, but will simply list their names. In particular, we recommend readers to be familiar with the following applications by checking the manuals therein: the "PSEUDO" module in the Bilbao Crystallographic Server (`https://www.cryst.ehu.es/cryst/pseudosymmetry.html`) and the "ISODISTORT" module in the ISOTROPY Software Suite (`https://stokes.byu.edu/iso/isodistort.php`), which provide possible choices for P_{high} based on giving P_{low} as input. In many cases, there are several different options for P_{high} (associated to P_{low}) and one has to select an appropriate P_{high} as the starting point. There are no general rules for such a selection. Which P_{high} to use depends on the specific physical questions. Given P_{high} and P_{low}, we can then compute the distortion modes characterizing P_{low} (with respect to P_{high}) by the "AMPLIMODES" module in the Bilbao Crystallographic Server (`https://www.cryst.ehu.es/cryst/amplimodes.html`) or the "ISODISTORT" module in the ISOTROPY Software Suite (`https://stokes.byu.edu/iso/isodistort.php`), and identify these modes as the relevant structural order parameters. We can also define the magnetic order parameters by assigning magnetic moments to the magnetically activate ions (e.g., $\mathbf{m}$ defined in Figure 1(h)). Notice that the order parameters are atomic motions or magnetic moments carried by ions

in the P_{high} phase, and should be transformed by the symmetry operations of P_{high}. We can get the generators of symmetry operations for P_{high} by the "GENPOS" module in the ISOTROPY Software Suite (`https://www.cryst.ehu.es/cryst/get_gen.html`). Having such information at hand, we shall define the transformations of each order parameter and form the energetic couplings following the aforementioned procedures.

2.3.6 A short summary

We have shown the basic principles for constructing energetic couplings for structural and magnetic order parameters in perovskites. In particular, for the coupling $\Pi_i r^{\mathbf{q_i}}_{Y_i,\alpha_i}$, $\sum_i q_{i\kappa}$ should be integer and magnetic order parameters should appear in couples, as required by translation and time-reversal symmetries, respectively. The rotation symmetry operations provide further constrains. We have also showcased how to construct some trilinear energetic couplings. Note, however, that even for the trilinear couplings there are many different possibilities to be considered, and that constructing a phenomenological theory can be quite difficult when starting from scratch. However, if one gains some information about which quantity couples to which (*e.g.*, from experiments or first-principles simulations) in advance, the development of the phenomenological theory may not be that complicated. In the next section, we will illustrate these ideas by reviewing some works introcuding various energetic couplings.

3 Some recently discovered energetic couplings

3.1 Structural distortions in orthorhombic perovskites

To begin with, let us emphasize that many ABX_3 perovskites (such as rare-earth orthoferrites[32] and orthochromites[33]) crystallize into the $Pbnm$ phase[23,34]. Starting from the $Pm\bar{3}m$ cubic perovskite, such a phase is achieved by condensing both in-phase and anti-phase tiltings of BX_6 octahedral (e.g., $(\omega_x^R, -\omega_y^R, \omega_z^{Mz})$ tilting pattern, as shown Figure 5). This $Pbnm$ phase additionally possesses anti-polar motions of the A ions along the x or y directions (see e.g., Refs.[35,36]), as shown in Figure 5(b). More precisely, there are two types of anti-polar motions for the A ions [22,23], namely those defined by $(u_{A,x}^{Xz}, -u_{A,y}^{Xz})$ and those associated with $(u_{A,x}^{R}, u_{A,y}^{R})$ in the symbolic language introduced in the present review (*cf* Figs. 6(a),(c)). These anti-polar motions were shown to be induced from anti-phase and in-phase tiltings of the BX_6 octahedral in, e.g., Refs.[22,23]. We now outline the basic ideas to obtain the corresponding energetic couplings.

Sketching the crystal structure of the $Pbnm$ phase in Figs. 5(a) and (b), it is easy to recognize its characteristic distortions (anti-phase tilting, in-phase tilting and anti-polar motions of A ions). The difficulty is how to relate the anti-polar motions to the in-phase and/or anti-phase tiltings. Incidentally, one may notice that for perovskites with only BX_6 anti-phase tilting (e.g., the $I4/mcm$ phase of $SrTiO_3$[37]) the anti-polar motions of A ions disappear[22] (see Figure 5(c)). Similarly, when only the in-phase BX_6 tilting is present, there are no anti-polar motions either[22]. This means that the *combination* of in-phase and anti-phase tiltings is a key factor driving the anti-polar motions of the A ions. Based on this observation, readers could proceed according to the principles for energetic couplings introduced in Section **2.3.1**.

For instance, the translation symmetry operations suggest the possibilities of having (i) a trilinear coupling among ω^R, ω^{Mz}, and u^{Xz}, and (ii) a quartic coupling among ω^R, ω^{Mz}, ω^{Mz}, and u^R, as low-order couplings. Let us, for instance, guess a trilinear term of the form $\omega_x^R\omega_z^{Mz}u_{A,x}^{Xz}$ and use Table 1 to proceed following the strategy mentioned in **2.3.4**. We find that $\omega_x^R\omega_z^{Mz}u_{A,x}^{Xz} \rightarrow \omega_x^R\omega_z^{Mz}u_{A,x}^{Xz}$ under 2_{001}, $\omega_x^R\omega_z^{Mz}u_{A,x}^{Xz} \rightarrow \omega_x^R\omega_z^{Mz}u_{A,x}^{Xz}$ by 2_{010}, $\omega_x^R\omega_z^{Mz}u_{A,x}^{Xz} \rightarrow \omega_y^R\omega_x^{Mx}u_{A,y}^{Xx}$ when applying 3^+_{111}, $\omega_x^R\omega_z^{Mz}u_{A,x}^{Xz} \rightarrow \omega_y^R\omega_z^{Mz}u_{A,y}^{Xz}$ due to 2_{110}, and $\omega_x^R\omega_z^{Mz}u_{A,x}^{Xz} \rightarrow \omega_x^R\omega_z^{Mz}u_{A,x}^{Xz}$ under $\bar{1}$, respectively. Our guessed terms are invariant under 2_{001}, 2_{010}, and $\bar{1}$. but not when applying 2_{110}, which rather suggests to inspect the combination $\omega_x^R\omega_z^{Mz}u_{A,x}^{Xz} + \omega_y^R\omega_z^{Mz}u_{A,y}^{Xz}$ – which can be written in a compact form as $\omega_{x\bar{y}}^R\omega_z^{Mz}u_{A,x\bar{y}}^{Xz}$, following the notation in Ref.[23]. Taking then 3^+_{111} into consideration, the full symmetry-allowed energetic coupling is $(\omega_x^R\omega_z^{Mz}u_{A,x}^{Xz} + \omega_y^R\omega_z^{Mz}u_{A,y}^{Xz}) + c.p.$ where $c.p.$ means cyclic permutations, e.g., $x \rightarrow y$, $y \rightarrow z$, $z \rightarrow x$

and $x \rightarrow z$, $y \rightarrow x$, $z \rightarrow y$. This coupling clearly shows why there are $u^{Xz}_{A,x}$ and $-u^{Xz}_{A,y}$ anti-polar motions in ABX_3 given the $(\omega^R_x, -\omega^R_y, \omega^{Mz}_z)$ tilting pattern. Similarly, readers may derive the quartic coupling $\omega^R_{x\bar{y}}\omega^{Mz}_z\omega^{Mz}_z u^R_{A,xy} + c.p.$ shown in Ref.[23], where $x\bar{y}$ means the direction along the $x-y$ direction.

It is worth emphasizing that the two couplings $\omega^R_{xy}\omega^{Mz}_z u^{Xz}_{A,xy}$ and $\omega^R_{xy}\omega^{Mz}_z\omega^{Mz}_z u^R_{A,x\bar{y}}$ are crucial for obtaining the so-called hybrid improper ferroelectricity in perovskite $ABX_3/A'BX_3$ superlattices[6,8]. For example, in Figure 6(a), the *Pbnm* phase of ABX_3 is antipolar (null polarization) because the A ions displace along the opposite direction (e.g., b and $-b$ for $u^{Xz}_{A,x\bar{y}}$) from one plane to another with precisely the same magnitude. However, when forming a $ABX_3/A'BX_3$ superlattice with the composition modulated along the direction of the in-phase tilts (see Figure 6(b)), A and A' displaced oppositely but with *different* magnitudes. Consequently, the $ABX_3/A'BX_3$ superlattice will exhibit an uncompensated polarization along the $-b$ or b direction for (001) 1×1 $ABX_3/A'BX_3$ superlattice. Interestingly, based on this hybrid improper ferroelectricity, one can design near-room temperature multiferroic superlattices, *e.g.* in La_2NiMnO_6/R_2NiMnO_6 (R being rare earth)[38]. It was also predicted that a five-state path resulting in the switching of polarization and magnetization under an electric field, via the reversal of anti-phase octahedral tiltings, can occur in some superlattices exhibiting hybrid improper ferroelectricity[39]. Here, we will not go through with so many details on hybrid improper ferroelectricity and its application, but refer interested readers to Refs.[5–8,38,39]. Nevertheless, we point to the fact that Ref.[40] numerically found that the phonon modes associated with polarization or antipolar motions in hybrid improper ferroelectrics can act rather unusually, namely they are hard in the high-temperature paraelectric phase (like in improper ferroelectrics[41,42]) while they soften on approaching the ferroelectric-to-paraelectric phase transition from below (as, in proper ferroelectrics). Such a unusual mixed behavior originates from the $\omega^R_{x\bar{y}}\omega^{Mz}_z u^{Xz}_{A,x\bar{y}}$ coupling, as also previously found in Ref.[43].

It is also worthwhile to indicate that Ref.[22] first looks for energetic couplings at an *atomistic* level, that is, involving the local displacement of a central A ion and the pseudo-vectors of its eight nearest B ions. Two energies were then found to be, having the following form:

$$\begin{aligned}
\Delta E_1 = K_1 \sum_i [&u_{A,i,z}(\omega_{i,1,y}\omega_{i,1,z} + \omega_{i,2,y}\omega_{i,2,z} + \omega_{i,5,y}\omega_{i,5,z} + \omega_{i,6,y}\omega_{i,6,z}) \\
&-u_{A,i,z}(\omega_{i,3,y}\omega_{i,3,z} + \omega_{i,4,y}\omega_{i,4,z} + \omega_{i,7,y}\omega_{i,7,z} + \omega_{i,8,y}\omega_{i,8,z}) \\
&+u_{A,i,z}(\omega_{i,1,x}\omega_{i,1,z} + \omega_{i,4,x}\omega_{i,4,z} + \omega_{i,5,x}\omega_{i,5,z} + \omega_{i,8,x}\omega_{i,8,z}) \\
&-u_{A,i,z}(\omega_{i,2,x}\omega_{i,2,z} + \omega_{i,3,x}\omega_{i,3,z} + \omega_{i,6,x}\omega_{i,6,z} + \omega_{i,7,x}\omega_{i,7,z})] \\
&+u_{A,i,x}(\omega_{i,1,x}\omega_{i,1,z} + \omega_{i,2,x}\omega_{i,2,z} + \omega_{i,3,x}\omega_{i,3,z} + \omega_{i,4,x}\omega_{i,4,z}) \\
&-u_{A,i,x}(\omega_{i,5,x}\omega_{i,5,z} + \omega_{i,6,x}\omega_{i,6,z} + \omega_{i,7,x}\omega_{i,7,z} + \omega_{i,8,x}\omega_{i,8,z}) \\
&+u_{A,i,x}(\omega_{i,1,x}\omega_{i,1,y} + \omega_{i,2,x}\omega_{i,2,y} + \omega_{i,5,x}\omega_{i,5,y} + \omega_{i,6,x}\omega_{i,6,y}) \\
&-u_{A,i,x}(\omega_{i,3,x}\omega_{i,3,y} + \omega_{i,4,x}\omega_{i,4,y} + \omega_{i,7,x}\omega_{i,7,y} + \omega_{i,8,x}\omega_{i,8,y}) \\
&+u_{A,i,y}(\omega_{i,1,x}\omega_{i,1,y} + \omega_{i,4,x}\omega_{i,4,y} + \omega_{i,5,x}\omega_{i,5,y} + \omega_{i,8,x}\omega_{i,8,y}) \\
&-u_{A,i,y}(\omega_{i,2,x}\omega_{i,2,y} + \omega_{i,3,x}\omega_{i,3,y} + \omega_{i,6,x}\omega_{i,6,y} + \omega_{i,7,x}\omega_{i,7,y}) \\
&+u_{A,i,y}(\omega_{i,1,z}\omega_{i,1,y} + \omega_{i,2,z}\omega_{i,2,y} + \omega_{i,3,z}\omega_{i,3,y} + \omega_{i,4,z}\omega_{i,4,y}) \\
&-u_{A,i,y}(\omega_{i,5,z}\omega_{i,5,y} + \omega_{i,6,z}\omega_{i,6,y} + \omega_{i,7,z}\omega_{i,7,y} + \omega_{i,8,z}\omega_{i,8,y})
\end{aligned} \tag{6}$$

and

$$
\begin{aligned}
\Delta E_2 = K_2 \sum_i [& u_{A,i,z}(\omega_{i,2,y}^2\omega_{i,2,z} + \omega_{i,4,y}^2\omega_{i,4,z} + \omega_{i,5,y}^2\omega_{i,5,z} + \omega_{i,7,y}^2\omega_{i,7,z}) \\
& -u_{A,i,z}(\omega_{i,1,y}^2\omega_{i,1,z} + \omega_{i,3,y}^2\omega_{i,3,z} + \omega_{i,6,y}^2\omega_{i,6,z} + \omega_{i,8,y}^2\omega_{i,8,z}) \\
& +u_{A,i,z}(\omega_{i,1,x}^2\omega_{i,1,z} + \omega_{i,3,x}^2\omega_{i,3,z} + \omega_{i,6,x}^2\omega_{i,6,z} + \omega_{i,8,x}^2\omega_{i,8,z}) \\
& -u_{A,i,z}(\omega_{i,2,x}^2\omega_{i,2,z} + \omega_{i,4,x}^2\omega_{i,4,z} + \omega_{i,5,x}^2\omega_{i,5,z} + \omega_{i,7,x}^2\omega_{i,7,z}) \\
& +u_{A,i,x}(\omega_{i,2,z}^2\omega_{i,2,x} + \omega_{i,4,z}^2\omega_{i,4,x} + \omega_{i,5,z}^2\omega_{i,5,x} + \omega_{i,7,z}^2\omega_{i,7,x}) \\
& -u_{A,i,x}(\omega_{i,1,z}^2\omega_{i,1,x} + \omega_{i,3,z}^2\omega_{i,3,x} + \omega_{i,6,z}^2\omega_{i,6,x} + \omega_{i,8,z}^2\omega_{i,8,x}) \\
& +u_{A,i,x}(\omega_{i,1,y}^2\omega_{i,1,x} + \omega_{i,3,y}^2\omega_{i,3,x} + \omega_{i,6,y}^2\omega_{i,6,x} + \omega_{i,8,y}^2\omega_{i,8,x}) \\
& -u_{A,i,x}(\omega_{i,2,y}^2\omega_{i,2,x} + \omega_{i,4,y}^2\omega_{i,4,x} + \omega_{i,5,y}^2\omega_{i,5,x} + \omega_{i,7,y}^2\omega_{i,7,x}) \\
& +u_{A,i,y}(\omega_{i,2,x}^2\omega_{i,2,y} + \omega_{i,4,x}^2\omega_{i,4,y} + \omega_{i,5,x}^2\omega_{i,5,y} + \omega_{i,7,x}^2\omega_{i,7,y}) \\
& -u_{A,i,y}(\omega_{i,1,x}^2\omega_{i,1,y} + \omega_{i,3,x}^2\omega_{i,3,y} + \omega_{i,6,x}^2\omega_{i,6,y} + \omega_{i,8,x}^2\omega_{i,8,y}) \\
& +u_{A,i,y}(\omega_{i,1,z}^2\omega_{i,1,y} + \omega_{i,3,z}^2\omega_{i,3,y} + \omega_{i,6,z}^2\omega_{i,6,y} + \omega_{i,8,z}^2\omega_{i,8,y}) \\
& -u_{A,i,y}(\omega_{i,2,z}^2\omega_{i,2,y} + \omega_{i,4,z}^2\omega_{i,4,y} + \omega_{i,5,z}^2\omega_{i,5,y} + \omega_{i,7,z}^2\omega_{i,7,y})
\end{aligned}
\tag{7}
$$

where $\omega_{i,m,\alpha}$ is the α-component of the tilting pseudo-vector associated with the m^{th} B ion surrounding A ion i (where m can range between 1 and 8, see Figure 3a), and this A ion displaces by $u_{A,i,\beta}$ along the β-direction.

Interesting, for the *Pbnm* structure, ΔE_1 and ΔE_2 precisely correspond to $(\omega_x^R\omega_z^{Mz}u_{A,x}^{Xz} + \omega_y^R\omega_z^{Mz}u_{A,y}^{Xz}) + c.p.$ and $\omega_{xy}^R\omega_z^{Mz}\omega_z^{Mz}u_{A,x\bar{y}}^R + c.p.$, respectively, when going from the atomic scale to a formula involving macroscopic order parameters. Strikingly, ΔE_1 and ΔE_2 can also be used to understand the occurrence of antipolar displacements originating from X octahedral tiltings in various other phases, as detailed in Table I of Ref.[22]. In particular, ΔE_1 naturally explains why long-period antipolar displacements can happen in the so-called nanotwin phases having a complex tilting patterns[44]. In such case, ω_x^R (respectively, ω_y^R) can interact with both $\omega_z^{\mathbf{q_1}}$ and $u_{A,x}^{\mathbf{q_2}}$ (respectively, $u_{A,y}^{\mathbf{q_2}}$), where $\mathbf{q_1} = (1/2, 1/2, \delta)$ and $\mathbf{q_2} = (0, 0, 1/2 - \delta)$, with δ between 0 and 1/2 ($\mathbf{q_1}$ is thus a q-point between M and R, while $\mathbf{q_2}$ is between X and Γ).

Note that such long-wave atomic arrangements can generate unusual phenomena, such as "pinched" hysteresis polarization-*versus*-electric field loop in defect-free materials[45]. Interestingly, the ΔE_1 coupling can also interact with other energetic couplings to provide novel physics. For instance, ΔE_1 has been found in Refs.[46,47] to be responsible for generating the *Pbcm* state of $NaNbO_3$, for which $\delta = 1/4$ and thus $\mathbf{q_1} = (1/2, 1/2, 1/4)$ is the T-point and $\mathbf{q_2} = (0, 0, 1/4)$ is the Δ-point. However, the existence of all these physical quantities also implies that another energetic coupling is activated, that is one coupling four order parameters, namely ω_x^R, ω_z^T, $u_{A,x}^{\Delta}$ and $u_{A,z}^{\Gamma}$, as well as an equivalent one coupling ω_y^R, ω_z^T, $u_{A,y}^{\Delta}$ and $u_{A,z}^{\Gamma}$. Consequently, a polarization appears along the z-axis (which is associated with $u_{A,z}^{\Gamma}$), which in fact transforms the antipolar *Pbcm* state into a polar one of symmetry $Pca2_1$. In other words, the existence of simultaneous energetic couplings leads to wondering if the room-temperature state of $NaNbO_3$ is not *Pbcm* but rather $Pca2_1$. Experiments are called for to check such recent prediction.

In summary, in this subsection we have illustrated the logic of how to guess a coupling and derive the associated phenomenological theory based on some previous information (e.g., crystal structures of *Pbnm* and related perovskites) or atomistic energies. We will now review other works on phenomenological theories involving phenomena such as: bilinear couplings between cation displacements and octahedral tiltings, spin and dipole canting, magnetically driven improper ferroelectricity, and some magnetoelectric couplings, taking perovskites as a platform. We will review some experimental facts and local interactions, and outline the ideas for deriving the energetic couplings, but (for the sake of brevity) omit the details on how to apply the symmetry operations. We will also provide two other sections dedicated to couplings generating electrical polarization and complex phenomena.

3.2 Bilinear couplings between cation displacements and octahedral tiltings

One may wonder if the aforementioned trilinear energetic coupling is the lowest in order when dealing with structural deformations. Surprisingly, it was found that there is an even lower order between cation displacements and octahedral tilings in perovskites[24]. It is a bilinear coupling that has the following atomistic form:

$$\begin{aligned}\Delta E_3 = K_3 \sum_i [&u_{A,i,x}(\omega_{i,1,y} + \omega_{i,2,y} + \omega_{i,3,y} + \omega_{i,4,y}) \\ &-u_{A,i,x}(\omega_{i,5,y} + \omega_{i,6,y} + \omega_{i,7,y} + \omega_{i,8,y}) \\ &+u_{A,i,y}(\omega_{i,5,x} + \omega_{i,6,x} + \omega_{i,7,x} + \omega_{i,8,x}) \\ &-u_{A,i,y}(\omega_{i,1,x} + \omega_{i,2,x} + \omega_{i,3,x} + \omega_{i,4,x}) \\ &+u_{A,i,y}(\omega_{i,1,z} + \omega_{i,4,z} + \omega_{i,5,z} + \omega_{i,8,z}) \\ &-u_{A,i,y}(\omega_{i,2,z} + \omega_{i,3,z} + \omega_{i,6,z} + \omega_{i,7,z}) \\ &+u_{A,i,z}(\omega_{i,2,y} + \omega_{i,3,y} + \omega_{i,6,y} + \omega_{i,7,y}) \\ &-u_{A,i,z}(\omega_{i,1,y} + \omega_{i,4,y} + \omega_{i,5,y} + \omega_{i,8,y}) \\ &+u_{A,i,z}(\omega_{i,1,x} + \omega_{i,2,x} + \omega_{i,5,x} + \omega_{i,6,x}) \\ &-u_{A,i,z}(\omega_{i,3,x} + \omega_{i,4,x} + \omega_{i,7,x} + \omega_{i,8,x}) \\ &+u_{A,i,x}(\omega_{i,3,z} + \omega_{i,4,z} + \omega_{i,7,z} + \omega_{i,8,z}) \\ &-u_{A,i,x}(\omega_{i,1,z} + \omega_{i,2,z} + \omega_{i,5,z} + \omega_{i,6,z})]\end{aligned} \tag{8}$$

Note that Ref.[24] also proposed that this ΔE_3 energy can be rewritten in the continuum limit by involving (real-space) curl of cation displacements coupled with tiltings, and *vice-versa* (i.e., real-space curl of tiltings coupled with cation displacements). Interestingly, Ref.[24] further demonstrated that two specific modes each provide a non-zero ΔE_3 local energetic coupling: one is the $\Sigma_2 = (1/4, 1/4, 0)$ mode and another is $S_4 = (1/4, 1/4, 1/2)$. In other words, these previously overlooked couplings can be used to explain the origin of the complex *Pbam* ground state of the prototype of antiferroelectrics, that is $PbZrO_3$, that has Σ_2 and S_4 modes[48–53]. In fact, these modes should be considered as hybrid, in the sense that they are made of a *mixture* of unusual cation displacements and octahedral tiltings, as consistent with Ref.[54]. Strikingly, the local bilinear coupling of Ref.[24] can also yield other complex structural arrangements, including those (i) indexed by the Λ_3 q-point defined as $(1/4, 1/4, 1/2)$ and responsible for a predicted $\sqrt{2}\times4\times\sqrt{2}$ phase of *Pnma* symmetry in $BiFeO_3$ and $Bi(Fe_{1/2}Sc_{1/2})O_3$ systems[55,56]; (ii) incommensurate phases known to occur in lead-based perovskites[57] for which the modulation has an irrational repetition period; and (iii) even the existence of an uncompensated polarization in incommensurate structural modulations of perovskite antiferroelectrics[58].

3.3 Spin and dipole canting in perovskites

Let us now recall that rare-earth orthoferrites $R FeO_3$[32] and orthochromites $R CrO_3$[33] adopt a *Pbnm* ground state (see, *e.g.*, Figs. 5(a) and (b)). The predominant antiferromagnetic (AFM) structures of the transition-metal (Fe^{3+} or Cr^{3+}) sublattice are termed as $G-$type, with an associated AFM vector pointing along the *a*, *b*, or *c* directions and denoted as G_a, G_b, or G_c (in our language, $m^R_{B,xy}$, $m^R_{B,\bar{x}y}$, or $m^R_{B,z}$, with B =Fe, Cr), respectively[11,59]. Because of the magnetic Dzyaloshinskii–Moriya interaction[60,61], spin canting occurs in $R FeO_3$ and $R CrO_3$ compounds; in particular, with G_a or G_c ordering, weak ferromagnetism appears with the magnetization direction being along *c* or *a* (say, $m^\Gamma_{B,z}$ or $m^\Gamma_{B,xy}$ in our language), respectively, which was both experimentally observed and theoretically confirmed (sketched in Figure 7)[9,11,59].

How to link the above experimental facts with symmetry-allowed energetic couplings? We can first notice that $R FeO_3$ and $R CrO_3$ are both ABX_3 perovskites with a $(\omega^R_x, -\omega^R_y, \omega^{Mz}_z)$ tilting pattern, and wonder if these octahedral rotations may be the driving force for spin canting. To check this, readers may employ first-principles techniques and conduct non-collinear magnetism calculations for ABX_3 compounds

with various tilting patterns and predominant $G-$type antiferromagnetic vectors along different directions. As shown in Ref.[9], in *e.g.*, $BiFeO_3$, when $G-$type antiferromagnetic vectors (on the Fe sublattice) and anti-phase FeO_6 tiltings are along two perpendicular directions, there appears a weak magnetic component along the third, orthogonal direction. Such "numerical experiments" strongly suggest a coupling involving ω_{α}^{R}, $m_{B,\beta}^{R}$, and $m_{B,\gamma}^{\Gamma}$ (B=Fe) with $\alpha \neq \beta \neq \gamma$, which is fully consistent with the $\boldsymbol{\omega}^{R} \cdot (\mathbf{m}_{B}^{R} \times \mathbf{m}_{B}^{\Gamma})$ energetic coupling derived in Section **2.3.4**.

Note that, in rare-earth orthoferrites and orthochromites, as indicated above, the anti-phase tilting corresponds to $\omega_{x\bar{y}}^{R}$, i.e., it is along the $-\mathbf{b}$ direction. As a result, the predominant AFM ordering, $m_{B,xy}^{R}$ (*i.e.*, G_a, along the **a** direction) or $m_{B,z}^{R}$ (*i.e.*, G_c, along the **c** direction), implies the occurrence of m_{z}^{Γ} and m_{xy}^{Γ}, which correspond to a weak ferromagnetic moment along the **c** and **a** directions, respectively. Hence, the $\boldsymbol{\omega}^{R} \cdot (\mathbf{m}_{B}^{R} \times \mathbf{m}_{B}^{\Gamma})$ energy coupling naturally explains the weak ferromagnetism (and associated spin canting) in rare-earth orthoferrites and orthochromites, and ascribes the structural origin of the Dzyaloshinskii–Moriya interaction to anti-phase tilting of FeO_6 or CrO_6 octahedra.

Furthermore, other energetic couplings (Eq. 9) regarding various kinds of magnetic structures have also been introduced in Refs.[9,12]. The whole set of these couplings is given by:

$$\begin{aligned}\Delta E_4 = {} & \eta \boldsymbol{\omega}^{R} \cdot (\mathbf{m}_{B}^{R} \times \mathbf{m}_{B}^{\Gamma}) + \xi \boldsymbol{\omega}^{R} \cdot (\mathbf{m}_{B}^{M} \times \mathbf{m}_{B}^{X}) + \chi \boldsymbol{\omega}^{M} \cdot (\mathbf{m}_{B}^{M} \times \mathbf{m}_{B}^{\Gamma}) \\ & + \zeta \boldsymbol{\omega}^{M} \cdot (\mathbf{m}_{B}^{R} \times \mathbf{m}_{B}^{X}) + \kappa \boldsymbol{\omega}^{R} \cdot (\mathbf{m}_{B}^{R} \times \mathbf{m}_{A}^{\Gamma}) + \lambda \boldsymbol{\omega}^{M} \cdot (\mathbf{m}_{B}^{M} \times \mathbf{m}_{A}^{\Gamma}) \end{aligned} \tag{9}$$

for which the M and X symbols should be understood as M_α and X_β, respectively, with α and β being determined according to the rules from translation symmetry (see Section **2.3.1**). η, ξ, χ, ζ, κ and λ are coefficients that characterize the strength of these interactions and are material dependent. Note also that Equation 9 naturally explains why the $R3c$ phase of bulk $BiFeO_3$, and the related Cc phases of $BiFeO_3$ films, can exhibit weak magnetism when their predominant magnetic order parameter is of G-type[62].

Strikingly, readers might notice that $\mathbf{u}_{B}^{R}$ transforms oppositely under $\bar{1}$ and $1'$ but identically under the rest of the generators, as compared with $\mathbf{m}_{B}^{R}$. This is also valid for $\mathbf{u}_{B}^{\Gamma}$ *versus* $\mathbf{m}_{B}^{\Gamma}$. In other words, $(\mathbf{u}_{B}^{R} \times \mathbf{u}_{B}^{\Gamma})$ and $(\mathbf{m}_{B}^{R} \times \mathbf{m}_{B}^{\Gamma})$ always transform identically under *all* symmetry operations. Hence, $\boldsymbol{\omega}^{R} \cdot (\mathbf{u}_{B}^{R} \times \mathbf{u}_{B}^{\Gamma})$ can be naturally obtained by simply generalizing $\boldsymbol{\omega}^{R} \cdot (\mathbf{m}_{B}^{R} \times \mathbf{m}_{B}^{\Gamma})$ to electric dipoles! This is quite important since the energy coupling $\boldsymbol{\omega}^{R} \cdot (\mathbf{u}_{B}^{R} \times \mathbf{u}_{B}^{\Gamma})$ indicates clearly the existence of a mechanism describing the possible canting of electric dipoles, as similar to Dzyaloshinskii–Moriya interaction describing the canting of magnetic moments. Reference[28] conducted first-principles calculations that did confirm the existence of this novel $\boldsymbol{\omega}^{R} \cdot (\mathbf{u}_{B}^{R} \times \mathbf{u}_{B}^{\Gamma})$ coupling energy in perovskites and coined it the "electric Dzyaloshinskii–Moriya interaction"[28] – to emphasize that it is the counterpart of the magnetic Dzyaloshinskii–Moriya interaction[60,61]. In fact, a detailed analysis proved the existence of twelve different mechanisms in perovskites, all involving octahedral tiltings, that are consistent with electric Dzyaloshinskii–Moriya interactions. For instance, the energy couplings in the electric regime, which form the electric counterpart of Eq. 9, is given by[28]

$$\begin{aligned}\Delta E_4' = {} & \eta' \boldsymbol{\omega}^{R} \cdot (\mathbf{u}_{B}^{R} \times \mathbf{u}_{B}^{\Gamma}) + \xi' \boldsymbol{\omega}^{R} \cdot (\mathbf{u}_{B}^{M} \times \mathbf{u}_{B}^{X}) + \chi' \boldsymbol{\omega}^{M} \cdot (\mathbf{u}_{B}^{M} \times \mathbf{u}_{B}^{\Gamma}) \\ & + \zeta' \boldsymbol{\omega}^{M} \cdot (\mathbf{u}_{B}^{R} \times \mathbf{u}_{B}^{X}) + \kappa' \boldsymbol{\omega}^{R} \cdot (\mathbf{u}_{B}^{R} \times \mathbf{u}_{A}^{\Gamma}) + \lambda' \boldsymbol{\omega}^{M} \cdot (\mathbf{u}_{B}^{M} \times \mathbf{u}_{A}^{\Gamma}) \end{aligned} \tag{10}$$

where η', ξ', χ', ζ', κ' and λ' are material-dependent parameters. In particular, and as discussed in Ref.[28], the terms associated wth χ' and λ' imply dipole cantings in perovskites possessing an in-phase tilting and a polarization whose directions are perpendicular to each other, and are at the heart of the inhomogeneous $Pmc2_1$ phase discovered in tensilely strained $BiFeO_3$[13,63,64], $PbTiO_3/BiFeO_3$ superlattices[65], and $RFeO_3$[66] (R being a rare earth). The occurrence of these latter two terms, along with the one associated with ζ in Eq. 9, was further found to induce an original magnetoelectric effect that makes it possible to control magnetism with an electric field[13]. As a matter of fact, switching the polarization in the $Pmc2_1$ state of $BiFeO_3$ first results in the change of the sense of the rotation of the in-phase oxygen octahedra, thanks to $\chi' \boldsymbol{\omega}^{M} \cdot (\mathbf{u}_{B}^{M} \times \mathbf{u}_{B}^{\Gamma})$ and $\lambda' \boldsymbol{\omega}^{M} \cdot (\mathbf{u}_{B}^{M} \times \mathbf{u}_{A}^{\Gamma})$. Then, this change in rotation induces the switching of the $\mathbf{m}_{B}^{X}$ antiferromagnetic vector, as governed by $\zeta \boldsymbol{\omega}^{M} \cdot (\mathbf{m}_{B}^{R} \times \mathbf{m}_{B}^{X})$. Note that other magnetoelectric effects can be designed by combining appropriate terms of Eqs. 9 and 10.

Let us also indicate that Ref.[28] further (i) derived six other energetic couplings that can also yield non-collinear electric dipolar configurations but that are not as simple as Dzyaloshinskii–Moriya interaction (that is, they do not involve a cross product between two electric quantities); and (ii) constructed a one-by-one correspondence between the magnetic and electric Dzyaloshinskii–Moriya interactions, strongly suggesting that physical quantities different from the oxygen octahedral tiltings can be at the heart of non-collinear electric dipolar arrangements. One obvious question for future studies is to determine what are these latter quantities, if any.

3.4 Magnetically-driven-ferroelectricity in perovskites with two magnetic sublattices

Let us illustrate the discusssion in this subsection by focusing on the $GdFeO_3$ perovskite. It has a *Pbnm* space group (*cf* Figure 5(a)[32]), and the Fe^{3+} and Gd^{3+} sublattices are magnetically ordered when temperatures are lower than 661 K and 2.5 K, respectively[15,67]. Interestingly, $GdFeO_3$ exhibits no polarization until *both* Fe^{3+} and Gd^{3+} adopt $G-$type ordering, as reported by Ref.[15]. The observed polarization is about 0.12 $\mu C/cm^2$, and oriented along the c-direction [15]. Such small value strongly hints at the fact that the polarization is of improper origin, and, in particular, may originate from the magnetic structures involving both Fe^{3+} and Gd^{3+} sublattices. It is clear that the predominant magnetic order for Fe^{3+} sublattice is $G-$type. However, because of the weak superexchange interaction between Gd^{3+} sites, the Gd^{3+} sublattice can be ordered in diverse ways, *e.g.*, with $G-$, $C-$, $A-$, or $F-$type orderings (see Ref.[26] for sketches) associated with R, M, X and Γ points defined in Figs. 3(a) and (b), respectively. One question to ask is thus: which magnetic order of Gd^{3+} sublattice can give rise to the polarization of $GdFeO_3$ and what is the responsible energy coupling?

A direct but tedious route to answer that is to start from the $G-$type ordering for Fe^{3+} along an α direction, and enumerate *all* the magnetic cases involving the Gd^{3+} sublattice, namely $G-$, $C-$, $A-$, or $F-$type orderings along β directions, with α and β being a, b, and c (as defined in Figs. 5(a),(b)). In total, 36 magnetic configurations can thus be considered and first-principles simulations using *non-collinear* magnetism can be performed on them, computing polarization along the way after structural relaxation are done. This is precisely what was done in Ref.[26]. Among the 36 cases, three were found to have a polarization of about 0.4 $\mu C/cm^2$ along the c direction, which is consistent with experiments[26]. All these three cases share the same characteristic, namely, Fe^{3+} and Gd^{3+} sublattices present a dual $G-$type ordering, with their resulting AFM vectors being aligned along the same direction. Such fact then motivated the authors of Ref.[26] to conduct additional computations, now using *collinear* magnetism. These additional calculations did find such a polarization, which strongly suggests that it does *not* originate from spin-orbit interactions. For instance, it is not a result of specific magnetic DMI effects, like the spin-curent model[68,69] valid for, e.g., $BiFeO_3$[70] and $TbMnO_3$[71].

Now, we aim at deriving the phenomenological theory for $GdFeO_3$ according to our above analysis. We know that the polarization is along the c-direction of the *Pbnm* phase (which is also our z-axis), and we thus pick $u^{\Gamma}_{B,z}$ from Table 1 since we are searching for a polarization. Note that it does not matter whether we consider $u^{\Gamma}_{B,z}$ or $u^{\Gamma}_{A,z}$, because they transform identically. We also now know that both Fe^{3+} and Gd^{3+} should be ordered as $G-$type along the same direction if we hope to induce a polarization. In our language, we pick the $\mathbf{m}^R_B$ and $\mathbf{m}^R_A$ quantities along the same direction (*e.g.*, $m^R_{B,x}$ and $m^R_{A,x}$). Naturally, we can form a coupling $m^R_{B,x}m^R_{A,x}u^{\Gamma}_{B,z}$ that fulfills the requirements from both translation and time-reversal symmetries. Unfortunately, $m^R_{B,x}m^R_{A,x}u^{\Gamma}_{B,z}$ is not a symmetry-allowed energetic coupling, because under the 2_{010} operation we have $m^R_{B,x}m^R_{A,x}u^{\Gamma}_{B,z} \rightarrow -m^R_{B,x}m^R_{A,x}u^{\Gamma}_{B,z}$. Before losing hope, we shall keep thinking about what was omitted so far. For instance, why not also taking the structural distortion (*e.g.*, in-phase and anti-phase tiltings) into consideration? For instance, what about a $\omega^R_x\omega^R_y m^R_{B,x}m^R_{A,x}u^{\Gamma}_{B,z}$ coupling, when realizing that the tilting pattern is $(\omega^R_x, -\omega^R_y, \omega^{Mz}_z)$ for *Pbnm* perovskite (see Section **3.1**) and that such a coupling is invariant when applying 2_{010} (as evidenced by looking at each involved physical quantity in this coupling under 2_{010} in Table 1). In fact, using *all* operation symmetries, it is straightforward to find that a symmetry-allowed energy coupling is $(\omega^R_x\omega^R_y m^R_{B,x}m^R_{A,x}u^{\Gamma}_{B,z} + \omega^R_x\omega^R_y m^R_{B,y}m^R_{A,y}u^{\Gamma}_{B,z}) + c.p.$. Similarly, starting from $\omega^R_x\omega^R_y m^R_{B,z}m^R_{A,z}u^{\Gamma}_{B,z}$ (for which the magnetic orderings are along the z-axis), we

can determine that $\omega_x^R\omega_y^R m_{B,z}^R m_{A,z}^R u_{B,z}^\Gamma + c.p.$ is another invariant. In fact, the collinear feature of the dual $G-$type magnetization of both Gd^{3+} and Fe^{3+} sublattices implies that we can involve $\mathbf{m}_B^R \cdot \mathbf{m}_A^R$. We thus arrive at $(\omega_x^R\omega_y^R u_{B,z}^\Gamma + \omega_y^R\omega_z^R u_{B,x}^\Gamma + \omega_z^R\omega_x^R u_{B,y}^\Gamma)\mathbf{m}_B^R \cdot \mathbf{m}_A^R$, which is precisely one energetic coupling derived in Ref.[26] to explain the occurrence of polarization in $GdFeO_3$. Note, however, that other mechanisms can result in a magnetically driven polarization in $GdFeO_3$ according to Ref.[26]. For example, the shear strain and anti-polar motions combining with $\mathbf{m}_B^R \cdot \mathbf{m}_A^R$ can give rise to polarization via the following couplings: $(\eta_{xy}u_{B,z}^\Gamma + \eta_{yz}u_{B,x}^\Gamma + \eta_{zx}u_{B,y}^\Gamma)\mathbf{m}_B^R \cdot \mathbf{m}_A^R$, $(u_{A,x}^R u_{A,y}^R u_{B,z}^\Gamma + u_{A,y}^R u_{A,z}^R u_{B,x}^\Gamma + u_{A,z}^R u_{A,x}^R u_{B,y}^\Gamma)\mathbf{m}_B^R \cdot \mathbf{m}_A^R$, and $(u_{A,x}^{Xz}u_{A,y}^{Xz}u_{B,z}^\Gamma + u_{A,y}^{Xx}u_{A,z}^{Xx}u_{B,x}^\Gamma + u_{A,z}^{Xy}u_{A,x}^{Xy}u_{B,y}^\Gamma)\mathbf{m}_B^R \cdot \mathbf{m}_A^R$, respectively (see Ref.[26] for details).

3.5 High-order Magnetoelectric couplings

Higher-order couplings can give rise to ever more complex effects that may be of interest, even for application. As an example, we briefly note an investigation of magnetoelectric couplings in $CaMnO_3$. Let us first recall that the perovskite $CaMnO_3$ has a $Pbnm$ symmetry and a predominant $G-$type magnetic ordering[72], similar to the case of rare-earth orthoferrites and orthochromites (see Figure 5(a)). Due to spin canting, it also shows weak ferromagnetism along the a or c directions when $G-$type magnetic vectors are along the c or a directions, respectively[72]. The underlying mechanism is similar to the one describing the spin canting in Section **3.3**. Morever, under tensile strain, $Pb2_1m$ and $P2_1mn$ phases have been predicted to happen, the latter being the ground state and the former being metastable[14,72]. Unlike the $Pbnm$ state, these two phases are polar with a polarization pointing along the b and a direction, respectively (see Figure 5(a)) for these directions). Furthermore, by applying electric field along the b direction, it should be possible to transform the $P2_1mn$ into the $Pb2_1m$ state. During the switch of the polarization from a to $-a$, b to $-b$ or a to b, the weak ferromagnetic moments are greatly changed, according to first-principles calculations; magnetoelectric coupling is thus demonstrated[14]. Interestingly, Ref.[14] determined that such magnetoelectric coupling is of high-order, namely of the form

$$\begin{aligned}\Delta E_5 = \gamma_1(&u_{B,x}^\Gamma u_{B,y}^\Gamma \omega_x^R m_x^R m_z^\Gamma + u_{B,y}^\Gamma u_{B,z}^\Gamma \omega_y^R m_y^R m_x^\Gamma + u_{B,z}^\Gamma u_{B,x}^\Gamma \omega_z^R m_z^R m_y^\Gamma \\ &- u_{B,x}^\Gamma u_{B,y}^\Gamma \omega_y^R m_y^R m_z^\Gamma - u_{B,y}^\Gamma u_{B,z}^\Gamma \omega_z^R m_z^R m_x^\Gamma - u_{B,z}^\Gamma u_{B,x}^\Gamma \omega_x^R m_x^R m_y^\Gamma) \\ +\gamma_2(&u_{B,x}^\Gamma u_{B,y}^\Gamma \omega_x^R m_z^R m_x^\Gamma + u_{B,y}^\Gamma u_{B,z}^\Gamma \omega_y^R m_x^R m_y^\Gamma + u_{B,z}^\Gamma u_{B,x}^\Gamma \omega_z^R m_y^R m_z^\Gamma \\ &- u_{B,x}^\Gamma u_{B,y}^\Gamma \omega_y^R m_z^R m_y^\Gamma - u_{B,y}^\Gamma u_{B,z}^\Gamma \omega_z^R m_x^R m_z^\Gamma - u_{B,z}^\Gamma u_{B,x}^\Gamma \omega_x^R m_y^R m_x^\Gamma)\end{aligned} \quad (11)$$

3.6 Other energy couplings involving electrical polarization

There are, in fact, a plethora of symmetry-allowed energy couplings that involve polarization. The aim of this section is to briefly mention some of them, putting an emphasis on their physical consequences.

For instance, one may wonder if, in addition to the couplings indicated in Sections 3.1 and 3.2, there are other energies involving both polar cation displacements and tilting of BX_6 octahedra. The answer is definitely yes, since the following bi-quadratic couplings are known to exist in perovskites[73]: $\omega_x^R\omega_x^R u_{A,x}^\Gamma u_{A,x}^\Gamma + c.p.$, $\omega_x^R\omega_x^R u_{B,x}^\Gamma u_{B,x}^\Gamma + c.p.$, $\omega_x^R\omega_x^R u_{A,y}^\Gamma u_{A,y}^\Gamma + c.p.$, $\omega_x^R\omega_x^R u_{B,y}^\Gamma u_{B,y}^\Gamma + c.p.$, $\omega_x^{Mx}\omega_x^{Mx} u_{A,x}^\Gamma u_{A,x}^\Gamma + c.p.$, $\omega_x^{Mx}\omega_x^{Mx} u_{B,x}^\Gamma u_{B,x}^\Gamma + c.p.$, $\omega_x^{Mx}\omega_x^{Mx} u_{A,y}^\Gamma u_{A,y}^\Gamma + c.p.$, $\omega_x^{Mx}\omega_x^{Mx} u_{B,y}^\Gamma u_{B,y}^\Gamma + c.p.$. Interestingly, these couplings were typically found to be *competitive* in nature, *e.g.*, a tilting occurring about an α-axis tends to annihilate the development of the polarization along such axis, and *vice-versa*[73,74].

On the other hand, there are other bi-quadratic couplings that are *collaborative* in nature. They are of the form, $\omega_x^R\omega_y^R u_{A,x}^\Gamma u_{A,y}^\Gamma + c.p.$, $\omega_x^R\omega_y^R u_{B,x}^\Gamma u_{B,y}^\Gamma + c.p.$, $\omega_x^{Mx}\omega_y^{My} u_{A,x}^\Gamma u_{A,y}^\Gamma + c.p.$ and $\omega_x^{Mx}\omega_y^{My} u_{B,x}^\Gamma u_{By}^\Gamma + c.p.$. Such couplings can, *e.g.*, explain why various phases possess a $R3c$ phase where polarization along $< 111 >$ pseudo-cubic directions coexist with tiltings about the same direction[73,74]. They may also induce novel phenomena such as a structural transition possessing several order parameters with none of them being primary, that is, a phase transition that is neither proper nor improper but rather of special trigger-type nature[74,75].

Even more surprising is the recent discovery of another collaborative high-order interaction in Ref.[76]. It is quadratic in cation displacements and quartic in tiltings, say $(u^{\Gamma}_{A,x}u^{\Gamma}_{A,x}+u^{\Gamma}_{A,y}u^{\Gamma}_{A,y}+u^{\Gamma}_{A,z}u^{\Gamma}_{A,z})(\omega^{R}_{x}\omega^{R}_{x}+\omega^{R}_{y}\omega^{R}_{y}+\omega^{R}_{z}\omega^{R}_{z})^2$. It can result in ferroelectricity induced by universal steric mechanisms, and induce unusual behavior, such as an enhancement of all the three Cartesian components of the electric polarization under hydrostatic pressure or compressive epitaxial strain. Such coupling appears to be important in ABX_6 perovskites with small A cations, such as $ZnSnO_3$[76].

There are also couplings between other quantities and polarization, in perovskites or non-perovskites. For instance, a Jahn-Teller distortion Q can interact with the electrical polarization P (e.g., u^{Γ}_{A} or u^{Γ}_{B}) in perovskites via, e.g., couplings of the form PQu^{M}_{A}[64] and $P^2Q\omega^{M}$[64] (notice that, for simplicity, we omit the details about the spatial directions associated with displacement u, tilting ω and the M point in these expressions). Such energy terms lead to an electric-field manipulation of Jahn-Teller effect, orbital ordering and magnetic orderings[64,77].

Furthermore, other original energy coupling were found in the so-called NH_4CdCl_3-type structures[78–84], which were also denoted as post-post-perovskite in Ref.[85]. This is a trilinear coupling involving the polar mode and two pseudo-Jahn Teller deformations, and has the potential to make some magnetic systems multiferroic – such as rare-earth manganites[85].

Another example: in hexagonal rare-earth ferrites, a symmetry-allowed energy involves the polarization and the so-called K_3 mode[86–88], via a term that is proportional to PK_3^3. It also results in a strengthening of the polarization under pressure, as a consequence of the natural pressure-induced increase of the amplitude of the K_3 mode[87].

Similarly, a polar $Pmc2_1$ phase was recently found from first-principles in some brownmillerite materials[89], with the associated electrical polarization originating from an original energy coupling that is linear in the polar mode, quadratic in another distortion associated with a Λ_3 mode and linear in a X_4^- mode. Due to such couplings, the resulting ferroelectricity can be considered to be of novel type, since it differs from previously reported proper, improper, hybrid improper, and triggered kinds.

As regards magnetoelectric effects, in addition to the mechanisms indicated in Sections 3.4 and 3.5, the electrical polarization, $\mathbf{P}$, can couple with magnetism via other ways. For instance, it was recently predicted that the polarization of 134-type $AA'_3B_4O_{12}$ perovskites, such as $LaMn_3Cr_4O_{12}$, can be induced thanks to three original and previously overlooked interaction terms for which other physical quantities mediate the coupling between G-type antiferromagnetic vectors[25]. These quantities are oxygen tiltings or shear strain, and the resulting couplings are given by[25]: $\Sigma_{\alpha,\beta,\gamma}|\epsilon_{\alpha\beta\gamma}|G^{\mathrm{Mn}}_{\alpha}G^{\mathrm{Cr}}_{\beta}P_{\gamma}$, $\omega^{M}\Sigma_{\alpha,\beta,\gamma}\epsilon_{\alpha\beta\gamma}G^{\mathrm{Mn}}_{\alpha}G^{\mathrm{Cr}}_{\beta}P_{\gamma}$, $(G^{\mathrm{Mn}}_{x}G^{\mathrm{Cr}}_{x}+G^{\mathrm{Mn}}_{y}G^{\mathrm{Cr}}_{y}+G^{\mathrm{Mn}}_{z}G^{\mathrm{Cr}}_{z})\Sigma_{\alpha,\beta,\gamma}|\epsilon_{\alpha\beta\gamma}|\eta_{\alpha,\beta}P_{\gamma}$, $\Sigma_{\alpha,\beta,\gamma}|\epsilon_{\alpha\beta\gamma}|G^{\mathrm{Mn}}_{\alpha}G^{\mathrm{Cr}}_{\beta}\eta_{\gamma\alpha}P_{\alpha}$, and $\Sigma_{\alpha,\beta,\gamma}|\epsilon_{\alpha\beta\gamma}|G^{\mathrm{Mn}}_{\alpha}G^{\mathrm{Cr}}_{\beta}\eta_{\beta\gamma}P_{\beta}$, where ω^M, P, η, and G are in-phase CrO_6 tilting, polarization, shear strain and magnetic orders (associated with Mn and Cr sublattices), respectively. $\epsilon_{\alpha\beta\gamma}$ (α, β, and γ being x, y, or z) is the Levi-Civita symbol whose value is 1 for $\alpha\beta\gamma$ being even permutation, -1 for odd permutation and 0 otherwise. Such energies explain why $LaMn_3Cr_4O_{12}$ has a polarization [90–95]. Note that, strictly speaking, $LaMn_3Cr_4O_{12}$ is not the same as the perovskites ABX_3. As a result, the order parameters defined in Table 1 can not be directly used for $LaMn_3Cr_4O_{12}$. Readers may treat it as an example to understand how to construct phenomenological theory for non-perovskite materials as shown in Section 2.3.5 and Ref.[25].

Another original magnetoelectric effect was found in the boracite family, explaining why electric-field control of magnetism can occur there[96], thanks to the coupling of the form $M_xM_yP_z+M_yM_zP_x+M_zM_xP_y$, where M and P are magnetization and polarization order parameters. Such magnetoelectric effect was further put in use to predict that the $LaSrMnOsO_6$ perovskite should be a near room-temperature and switchable multiferroic, having rather large ferroelectric polarization and spontaneous magnetization as well as strong magnetoelectric coupling [96].

Moreover, the first-principles calculations of Refs.[97–99] predicted the occurrence of an electrical polarization near *magnetic* domain walls in both perovskites and rare-earth iron garnets, via a so-called symmetric exchange-striction mechanism. This effect implies that $\mathbf{P}$ can be written as $\sum_{<i,j>}\mathbf{P^{i,j}_{ex}}\,\mathbf{S_i}\cdot\mathbf{S_j}$, where the summation is over all the spin pairs and $\mathbf{P^{i,j}_{ex}}$ is the polarization coefficient vector associated with the $<i,j>$ spin pair[97,98].

The electrical polarization, $\mathbf{P}$, can also play a role as part of the magnetic DMI vector, via the energy

provided by the spin-current model[68,69]: $C(\mathbf{P}\times\mathbf{e_{ij}})\cdot(\mathbf{m_i}\times\mathbf{m_j})$, where C is a coefficient and $\mathbf{e_{ij}}$ is the unit vector joining the sites i and j, which possess the local magnetic moments $\mathbf{m_i}$ and $\mathbf{m_j}$, respectively. This spin-current model has been recently used to model and understand magnetic cycloids of the multiferroic $BiFeO_3$ perovskites[100–103], in general, and to predict that one can make a right-handed cycloid becoming left-handed (or *vice-versa*) by applying an electric field[104], in particular.

It is also important to mention that several physical quantities, including non-trivial ones, can simultaneously interact with each other, giving rise to interesting phenomena. For instance, Ref.[105] revealed, via first-principles calculations and their analysis, that one can control magnetization, Jahn-Teller distortion and orbital ordering via an electric field in some ferroelectric ferromagnets. This is because of three different types of energetic coupling: one coupling polarization with anti-phase and in-phase oxygen octahedral tiltings $P_x\omega_x^R\omega_z^{Mz}$ and $P_y\omega_y^R\omega_z^{Mz}$, a second one coupling polarization with anti-phase oxygen octahedra tilting and Jahn-Teller distortions $P_x\omega_x^R Q_z$ and $P_y\omega_y^R Q_z$, and finally a biquadratic coupling between anti-phase oxygen octahedral tilting and magnetization $\omega_x^R\omega_y^R m_{B,x}^{\Gamma}m_{B,y}^{\Gamma}$. Of comparable complexity was the recent prediction that an electric-field (E) can switch magnetic topological charge (Q) in a controllable and reversible fashion in some Type-I multiferroics[106]. This mechanism happens through the mediation of electric polarization (P) and Dzyaloshinskii-Moriya interaction (D), and was coined $EPDQ$.

3.7 Some "exotic" energetic couplings

Regarding topology, electrical topological defects can also occur, in addition to magnetic ones. For instance, electrical vortices, nanobubbles, dipolar waves, disclinations and skyrmions were predicted[107–112] and recently experimentally confirmed[110,113–116]. Such complex arrangements can have their own order parameter, such as the so-called electrical toroidal moment $\mathbf{T_E}$ for polar vortices, which consists of averaging the cross product of local electric dipoles with position of these dipoles over the whole system[107]. These "exotic" order parameters can, in principle, couple with other physical quantity, and generate novel effects. Of particular importance may be the coupling of the electrical toroidal moment with polarization and strain which are of the general form (when also incorporating coupling between polarization and strains): $\Sigma_{ijkl}(\zeta_{ijkl}T_{E,i}T_{E,j}\eta_{kl}+\lambda_{ijkl}T_{E,i}T_{E,j}P_kP_l+q_{ijkl}P_iP_j\eta_{kl})+\Sigma_i h_i T_{E,i}$ with h_i being the $T_{E,i}$'s conjugate field (that is, the curl of the electric field)[117]. Such couplings were predicted to (i) make the materials spontaneously optically active; and (ii) allow the systems to transform from their dextrorotatory to laevorotatory forms (and *vice-versa*) via the application of an electric field. Optical rotation of polarized light, as characterized by gyrotropic coefficients, was further found to be possibly maximized at room temperature by such application too, thanks to these couplings[118].

The electrical toroidal moment can also interact with BX_6 octahedral tiltings, in analogy to the biquadratic coupling between polarization and the tiltings indicated in Section 3.6. Such coupling can induce unusual patterns of these tiltings according to Ref.[119]. It can also generate novel phenomena: applying the *curl* of an electric field along some specific directions to a system with a predominant G-type antiferromagnetic vector can rotate $\mathbf{T_E}$ and, thus, also the axis about which BX_6 octahedra tilt in anti-phase fashion (because the electrical toroidal moment couples with these tiltings). This, in turn, makes the weak magnetization rotate (because of a tilting-driven DMI indicated in Eq. 9). In other words, applying curled electric fields can result in a control of the direction of the magnetization (note that it can also result in controlling the magnitude of the magnetization for other directions of the curled electric fields). This constitutes what was coined the "magnetotoroidic" effect in Ref.[120].

Other subtle interactions can also involve $\mathbf{T_E}$. For instance, it can interact with zero-point atomic vibrations in some specific systems, such as $KTaO_3$ dots, effectively annihilating the electrical toroidal moment[120]. Such a vanishing is reminiscent of the quantum-induced annihilation of the electrical polarization in systems known as incipient ferroelectrics[121]. Hence the name "incipient ferrotoroidics" given to materials like $KTaO_3$ dots in Ref.[122]. Note also that, as indicated in Ref.[123], *time-dependent* electrical toroidal moment has the dimension of a magnetic moment and can also be expressed as a product of the polarization and its time derivative. Consequently, Ref.[123] predicted that pulses of magnetization can occur in nominally nonmagnetic systems, if they adopt nanoscale ferroelectric domains that are moving

under the application of a GHz electric field. These striking magnetoelectric effects are, in fact, consistent with those observed and interpreted starting in the 1980's in Refs.[124–128].

Let us finish this presentation of "exotic" couplings by mentioning an energy that was first proposed based on symmetry arguments alone[69]. It is of the form: $\mathcal{E} = -\frac{a}{2}\int (\mathbf{r} \times (\mathbf{E} \times \mathbf{H})) \cdot \mathcal{M}(\mathbf{r})\, d^3r$, where a is a material-dependent constant, $\mathbf{r}$ is the position vector, $\mathbf{E}$ and $\mathbf{H}$ are electric and magnetic fields, respectively, and $\mathcal{M}(\mathbf{r})$ is the magnetization field. Such an energy can be considered as the coupling between the electromagnetic angular momentum density and magnetic moments, and was accordingly coined "AME for Angular MagnetoElectric coupling" in Ref.[129]. It was later found to originate from the relativistic Dirac equation, and, in fact, completes the traditional spin-orbit interaction by making the sum of the two interactions gauge-invariant (neither the traditional spin-orbit Hamiltonian nor the AME Hamiltonian is gauge invariant by itself)[130]. Very surprisingly, this AME energetic coupling was found to reproduce in a straightforward manner (i.e., via simple analytical derivations) the spin-current model[69], anomalous Hall effect[131–133], anisotropic magnetoresistance and planar Hall effects[134,135], interface-driven Rashba-Edelstein effects[136–138], inverse Faraday effect[130,139–142], and some uncommon spin-orbit-driven spin-torque terms[143–147]. This AME interaction may be further put in use to understand other complex phenomena or even perhaps design novel ones.

4 Summary

Using perovskite as a model system, we have shown how to define the order parameters, to obtain their transformations, and to derive symmetry-invariant energetic couplings. In particular, we have reviewed some previous works dealing with energetic couplings for perovskites and describing e.g., structural distortions, spin (dipole) cantings and magnetically driven ferroelectricity.

Let us briefly summarize the basic principles and procedures that allow us to deduce such energetic couplings. First, readers should notice that, when deriving energetic couplings, one has to define the order parameters and the transformations under symmetry operations. For this purpose, the target phase (e.g., phase to be investigated) and a high-symmetric reference phase are both needed; the order parameter (characterizing the target phase) and its transformation properties are defined with respect to the reference phase. Then, the principle to obtain energy couplings is that the interaction terms involving various order parameters, $\Pi_i r^{q_i}_{Y_i,\alpha_i}$, must be invariant under *all* the symmetry operations of the reference phase (i.e., translation, time-reversal, rotation symmetry operations). There are many possible couplings to find, but the constraints by translation and time-reversal symmetries drastically reduce the number of possible invariants, and the rotation symmetry further restricts the energetic couplings. Hence, the task of identifying the specific ones connected to experimental phenomena gets much simplified.

To determine the energetic couplings, one basically proceeds as follows:

- Based on the target phase, find its high-symmetric reference phase, a phase from which the target phase can be reached by reducing the symmetry (*e.g.*, phase transition).
- Define the order parameters relating the reference and target phases. The order parameters may be related to either structural distortions or magnetic arrangements.
- Find the generators of the symmetry operations of the reference phase and identify the transformations of the order parameters according to these generators.
- Link each order parameter with its $q-$point (in the first Brillouin zone) according to its transformation by lattice translations (listed in the set of generators).
- Guess a coupling involving the relevant order parameters. The translational symmetry requires the sum of the $q-$points (of the order parameters involved in the energy coupling) to be a reciprocal lattice $\mathbf{G}$ vector. The time-reversal symmetry requires the magnetism-related order parameters to have a total even power.

- Verify that the guessed coupling does not "disappear" by rotation symmetry operations. If it does, this coupling is not a symmetry invariant; hence, go back to the previous step and consider a new coupling. If the coupling does not disappear, find its corresponding "closed" form and verify that it is indeed an energetic coupling. For the meaning of "closed", see Sections **2.3.3** and **2.3.4**.

- Try linking the derived energetic coupling with the experimental phenomena, or make your prediction (and verify it) according to the energetic coupling.

Indeed, the derivation of a phenomenological theory is not an easy task. It usually requires trial and error by deeply considering the information at hand, such as experimental measurements and/or first-principles calculated data. An alternative way to generate the energy couplings is to use the INVARIANTS module in the ISOTROPY Software Suite (`https://stokes.byu.edu/iso/invariants.php`). Interested readers might check the manual, verify the energetic couplings mentioned in the above sections, and generate their own invariants.

Before we conclude we should stress that, while in this article we have discussed a large variety of couplings and effects, our compilation is by no means exhaustive. Indeed, particularly in recent years, there are plenty of examples of interesting multi-functional couplings and ever-more-complex phenomena being discussed in the literature. One especially interesting category relates to the effects associated to spatial gradients of the ferroic order parameters (e.g., flexoelectric couplings), which would warrant a review of their own. We refer the interested reader to Refs.[148–151] to get a feeling of the recent developments on that front.

We should also emphasize that another all-important aspect: When one develops a phenomenological theory to explain a set of experimental or computational data, one typically aims at identifying the simplest model (simplest energy couplings) that are able to account for the data. However, achieving this does not necessarily imply that the identified simple theory is correct; indeed, new data could prove it incomplete and requiring an extension. The case of $PbZrO_3$ is a likely example of this. The trilinear and harmonic couplings discussed, respectively, in Refs.[48] and[24] offer a plausible explanation for the stability of the observed ground state of the compound. However, new first-principles data point at the possible key role of other flexoelectric-like couplings[152] of the type introduced in Ref.[151], suggesting that a refined theory is needed. This "need for refinement" can potentially apply to all the specific examples presented here.

In sum, we hope that the techniques described in this crash course, and the cited softwares, will provide some assistance for researchers in the development of phenomenological theories tackling (multi)functional effects in ferroic materials. We also hope that the sections in which we review work on specific couplings and effects may be of interest to scientists working on these ever-surprising compounds.

Acknowledgements

The sketches were prepared by a combination of VESTA[153] and Mathematica[154] softwares. H. Z., C.P, K.P. and L.B. thank the Vannevar Bush Faculty Fellowship (VBFF) Grant No. N00014-20-1-2834 from the Department of Defense. P.C., S.P. and L.B. acknowledge the Office of Naval Research for the support under Grants No. N00014-17- 1-2818 and No. N00014-21-1-2086. J.I. thanks Grant FNR/C18/MS/12705883 "REFOX" from the Luxembourg National Research Fund.

References

[1] D. Damjanovic, P. Muralt, N. Setter, *IEEE Sensors Journal* **2001**, *1*, 3 191.

[2] W. Eerenstein, N. D. Mathur, J. F. Scott, *Nature* **2006**, *442*, 7104 759.

[3] J. F. Scott, *Nat. Mater.* **2007**, *6*, 4 256.

[4] E. Bousquet, M. Dawber, N. Stucki, C. Lichtensteiger, P. Hermet, S. Gariglio, J.-M. Triscone, P. Ghosez, *Nature* **2008**, *452*, 7188 732.

[5] N. A. Benedek, C. J. Fennie, *Phys. Rev. Lett.* **2011**, *106* 107204.

[6] J. M. Rondinelli, C. J. Fennie, *Adv. Mater.* **2012**, *24*, 15 1961.

[7] A. T. Mulder, N. A. Benedek, J. M. Rondinelli, C. J. Fennie, *Adv. Funct. Mater.* **2013**, 4810–4820.

[8] H. J. Zhao, J. Íñiguez, W. Ren, X. M. Chen, L. Bellaiche, *Phys. Rev. B* **2014**, *89* 174101.

[9] L. Bellaiche, Z. Gui, I. A. Kornev, *J. Phys.: Condens. Matter* **2012**, *24*, 31 312201.

[10] E. Bousquet, A. Cano, *J. Phys.: Condens. Matter* **2016**, *28*, 12 123001.

[11] R. L. White, *J. Appl. Phys.* **1969**, *40*, 3 1061.

[12] H. J. Zhao, J. Íñiguez, X. M. Chen, L. Bellaiche, *Phys. Rev. B* **2016**, *93* 014417.

[13] Y. Yang, J. Íñiguez, A.-J. Mao, L. Bellaiche, *Phys. Rev. Lett.* **2014**, *112* 057202.

[14] H. J. Zhao, M. N. Grisolia, Y. Yang, J. Íñiguez, M. Bibes, X. M. Chen, L. Bellaiche, *Phys. Rev. B* **2015**, *92* 235133.

[15] Y. Tokunaga, N. Furukawa, H. Sakai, Y. Taguchi, T. h. Arima, Y. Tokura, *Nat. Mater.* **2009**, *8*, 7 558.

[16] S. Dong, J.-M. Liu, S.-W. Cheong, Z. Ren, *Adv. Phys.* **2015**, *64*, 5-6 519.

[17] K. Wang, J.-M. Liu, Z. Ren, *Adv. Phys.* **2009**, *58*, 4 321.

[18] C. Lu, M. Wu, L. Lin, J.-M. Liu, *Natl. Sci. Rev.* **2019**, *6*, 4 653.

[19] M. Fiebig, T. Lottermoser, D. Meier, M. Trassin, *Nat. Rev. Mater.* **2016**, *1*, 8 16046.

[20] N. A. Spaldin, R. Ramesh, *Nat. Mater.* **2019**, *18*, 3 203.

[21] L. W. Martin, A. M. Rappe, *Nat. Rev. Mater.* **2016**, *2*, 2 16087.

[22] L. Bellaiche, J. Íñiguez, *Phys. Rev. B* **2013**, *88* 014104.

[23] P. Chen, M. N. Grisolia, H. J. Zhao, O. E. González-Vázquez, L. Bellaiche, M. Bibes, B.-G. Liu, J. I. niguez, *Phys. Rev. B* **2018**, *97* 024113.

[24] K. Patel, S. Prosandeev, Y. Yang, B. Xu, J. Íñiguez, L. Bellaiche, *Phys. Rev. B* **2016**, *94*, 5 054107.

[25] H. J. Zhao, P. Chen, S. Artyukhin, L. Bellaiche, *Phys. Rev. B* **2020**, *101* 214441.

[26] H. J. Zhao, L. Bellaiche, X. M. Chen, J. Íñiguez, *Nat. Commun.* **2017**, *8*, 1 14025.

[27] M. E. Lines, A. M. Glass, *Principles and Applications of Ferroelectrics and Related Materials*, Oxford University Press, **2001**.

[28] H. J. Zhao, P. Chen, S. Prosandeev, S. Artyukhin, L. Bellaiche, *Nat. Mater.* **2021**, *20*, 3 341.

[29] A. W. Joshi, *Elements of Group Theory for Physicists*, Wiley Eastern, **1984**.

[30] S. Cao, L. Chen, W. Zhao, K. Xu, G. Wang, Y. Yang, B. Kang, H. Zhao, P. Chen, A. Stroppa, R.-K. Zheng, J. Zhang, W. Ren, J. Íñiguez, L. Bellaiche, *Sci. Rep.* **2016**, *6*, 1 37529.

[31] S. J. Yuan, W. Ren, F. Hong, Y. B. Wang, J. C. Zhang, L. Bellaiche, S. X. Cao, G. Cao, *Phys. Rev. B* **2013**, *87*, 18 184405.

[32] M. Marezio, J. P. Remeika, P. D. Dernier, *Acta Crystallogr. B: Struct. Cryst. Cryst. Chem.* **1970**, *26*, 12 2008.

[33] J.-S. Zhou, J. A. Alonso, V. Pomjakushin, J. B. Goodenough, Y. Ren, J.-Q. Yan, J.-G. Cheng, *Phys. Rev. B* **2010**, *81*, 21 214115.

[34] M. W. Lufaso, P. M. Woodward, *Acta Crystallogr. B* **2001**, *57*, 6 725.

[35] H. J. Zhao, W. Ren, Y. Yang, X. M. Chen, L. Bellaiche, *J. Phys.: Condens. Matter* **2013**, *25*, 46 466002.

[36] H. J. Zhao, W. Ren, X. M. Chen, L. Bellaiche, *J. Phys.: Condens. Matter* **2013**, *25*, 38 385604.

[37] W. Jauch, A. Palmer, *Phys. Rev. B* **1999**, *60* 2961.

[38] H. J. Zhao, W. Ren, Y. Yang, J. Íñiguez, X. M. Chen, L. Bellaiche, *Nat. Commun.* **2014**, *5*, 1 4021.

[39] B. Xu, D. Wang, H. J. Zhao, J. Íñiguez, X. M. Chen, L. Bellaiche, *Adv. Funct. Mater.* **2015**, *25*, 24 3626.

[40] K. Patel, S. Prosandeev, B. Xu, L. Bellaiche, *Phys. Rev. B* **2019**, *100*, 21 214107.

[41] A. P. Levanyuk, D. G. Sannikov, *Usp. Fiz. Nauk* **1974**, *112* 561.

[42] W. Kaczmarek, F. Gervaid, *Ferroelectrics* **1988**, *80* 197.

[43] K. Patel, S. Prosandeev, L. Bellaiche, *npj Comput. Mater.* **2017**, *3*, 1 34.

[44] S. Prosandeev, D. Wang, W. Ren, J. Íñiguez, L. Bellaiche, *Adv. Funct. Mater.* **2012**, *23*, 2 234.

[45] B. Xu, C. Paillard, B. Dkhil, L. Bellaiche, *Phys. Rev. B* **2016**, *94*, 14 140101(R).

[46] Y. Yang, B. Xu, C. Xu, W. Ren, L. Bellaiche, *Phys. Rev. B* **2018**, *97*, 17 174106.

[47] K. Patel, S. Prosandeev, B. Xu, C. Xu, L. Bellaiche, *Phys. Rev. B* **2021**, *103*, 9 094103.

[48] J. Íñiguez, M. Stengel, S. Prosandeev, L. Bellaiche, *Phys. Rev. B* **2014**, *90*, 22 220103(R).

[49] S. Prosandeev, C. Xu, R. Faye, W. Duan, H. Liu, B. Dkhil, P.-E. Janolin, J. Íñiguez, L. Bellaiche, *Phys. Rev. B* **2014**, *89*, 21 214111.

[50] J. Hlinka, T. Ostapchuk, E. Buixaderas, C. Kadlec, P. Kuzel, I. Gregora, J. Kroupa, M. Savinov, A. Klic, J. Drahokoupil, I. Etxebarria, J. Dec, *Phys. Rev. Lett.* **2014**, *112*, 19 197601.

[51] E. Cockayne, K. Rabe, *J. Phys. Chem. Solids* **2000**, *61*, 2 305.

[52] B. K. Mani, S. Lisenkov, I. Ponomareva, *Phys. Rev. B* **2015**, *91*, 13 134112.

[53] B. Xu, O. Hellman, L. Bellaiche, *Phys. Rev. B* **2019**, *100*, 2 020102(R).

[54] P. Ghosez, E. Cockayne, U. V. Waghmare, K. M. Rabe, *Phys. Rev. B* **1999**, *60*, 2 836.

[55] S. A. Prosandeev, D. D. Khalyavin, I. P. Raevski, A. N. Salak, N. M. Olekhnovich, A. V. Pushkarev, Y. V. Radyush, *Phys. Rev. B* **2014**, *90* 054110.

[56] D. D. Khalyavin, A. N. Salak, N. M. Olekhnovich, A. V. Pushkarev, Y. V. Radyush, P. Manuel, I. P. Raevski, M. L. Zheludkevich, M. G. S. Ferreira, *Phys. Rev. B* **2014**, *89* 174414.

[57] G. Baldinozzi, P. Sciau, A. Bulou, *J. Phys.: Condens. Matter* **1997**, *9*, 47 10531.

[58] T. Ma, Z. Fan, B. Xu, T.-H. Kim, P. Lu, L. Bellaiche, M. J. Kramer, X. Tan, L. Zhou, *Phys. Rev. Lett.* **2019**, *123* 217602.

[59] B. Rajeswaran, D. I. Khomskii, A. K. Zvezdin, C. N. R. Rao, A. Sundaresan, *Phys. Rev. B* **2012**, *86*, 21 214409.

[60] I. E. Dzyaloshinskii, *Sov. Phys. JETP* **1957**, *5* 1259.

[61] T. Moriya, *Phys. Rev.* **1960**, *120*, 1 91.

[62] D. Albrecht, S. Lisenkov, W. Ren, D. Rahmedov, I. A. Kornev, L. Bellaiche, *Phys. Rev. B* **2010**, *81* 140401.

[63] Y. Yang, W. Ren, M. Stengel, X. H. Yan, L. Bellaiche, *Phys. Rev. Lett.* **2012**, *109* 057602.

[64] J. Varignon, N. C. Bristowe, P. Ghosez, *Phys. Rev. Lett.* **2016**, *116*, 5 057602.

[65] Y. Yang, M. Stengel, W. Ren, X. H. Yan, L. Bellaiche, *Phys. Rev. B* **2012**, *86* 144114.

[66] H. J. Zhao, Y. Yang, W. Ren, A.-J. Mao, X. M. Chen, L. Bellaiche, *J. Phys.: Condens. Matter* **2014**, *26*, 47 472201.

[67] D. Treves, *J. Appl. Phys.* **1965**, *36*, 3 1033.

[68] H. Katsura, N. Nagaosa, A. V. Balatsky, *Phys. Rev. Lett.* **2005**, *95* 057205.

[69] A. Raeliarijaona, S. Singh, H. Fu, L. Bellaiche, *Phys. Rev. Lett.* **2013**, *110* 137205.

[70] D. Rahmedov, D. Wang, J. Íñiguez, L. Bellaiche, *Phys. Rev. Lett.* **2012**, *109* 037207.

[71] A. Malashevich, D. Vanderbilt, *Phys. Rev. Lett.* **2008**, *101* 037210.

[72] E. Bousquet, N. Spaldin, *Phys. Rev. Lett.* **2011**, *107*, 19 197603.

[73] I. A. Kornev, L. Bellaiche, P.-E. Janolin, B. Dkhil, E. Suard, *Phys. Rev. Lett.* **2006**, *97* 157601.

[74] I. A. Kornev, L. Bellaiche, *Phys. Rev. B* **2009**, *79* 100105.

[75] J. Holakovský, *physica status solidi (b)* **1973**, *56*, 2 615.

[76] T. Gu, T. Scarbrough, Y. Yang, J. Íñiguez, L. Bellaiche, H. J. Xiang, *Phys. Rev. Lett.* **2018**, *120* 197602.

[77] J. Varignon, N. C. Bristowe, E. Bousquet, P. Ghosez, *Sci. Rep.* **2015**, *5*, 1 15364.

[78] R. Lelieveld, D. J. W. Ijdo, *Acta Crystallogr. B: Struct. Cryst. Cryst. Chem.* **1978**, *34*, 11 3348.

[79] A. Meetsma, G. A. Wiegers, J. L. de Boer, *Acta Crystallogr. C: Cryst. Struct. Commun.* **1993**, *49*, 12 2060.

[80] C.-S. Lee, K. M. Kleinke, H. Kleinke, *Solid State Sci.* **2005**, *7*, 9 1049.

[81] G. A. Wiegers, A. Meetsma, R. J. Haange, J. L. de Boer, *Acta Crystallogr. C: Cryst. Struct. Commun.* **1989**, *45*, 6 847.

[82] J. A. Brehm, J. W. Bennett, M. R. Schoenberg, I. Grinberg, A. M. Rappe, *J. Chem. Phys.* **2014**, *140*, 22 224703.

[83] W.-J. Yin, T. Shi, Y. Yan, *Adv. Mater.* **2014**, *26*, 27 4653.

[84] I. Chung, J.-H. Song, J. Im, J. Androulakis, C. D. Malliakas, H. Li, A. J. Freeman, J. T. Kenney, M. G. Kanatzidis, *J. Am. Chem. Soc.* **2012**, *134*, 20 8579.

[85] C. Xu, B. Xu, Y. Yang, H. Dong, A. R. Oganov, S. Wang, W. Duan, B. Gu, L. Bellaiche, *Phys. Rev. B* **2015**, *91* 020101.

[86] H. Das, A. L. Wysocki, Y. Geng, W. Wu, C. J. Fennie, *Nat. Commun.* **2014**, *5*, 1 2998.

[87] C. Xu, Y. Yang, S. Wang, W. Duan, B. Gu, L. Bellaiche, *Phys. Rev. B* **2014**, *89* 205122.

[88] F. Liu, C. Xu, S. Shen, N. Li, H. Guo, X. Lü, H. Xiang, L. Bellaiche, J. Zhao, L. Yin, W. Yang, W. Wang, J. Shen, *Phys. Rev. B* **2019**, *100* 214408.

[89] H. Tian, X.-Y. Kuang, A.-J. Mao, Y. Yang, H. Xiang, C. Xu, S. O. Sayedaghaee, J. Íñiguez, L. Bellaiche, *Phys. Rev. Materials* **2018**, *2* 084402.

[90] X. Wang, Y. Chai, L. Zhou, H. Cao, C. d. Cruz, J. Yang, J. Dai, Y. Yin, Z. Yuan, S. Zhang, R. Yu, M. Azuma, Y. Shimakawa, H. Zhang, S. Dong, Y. Sun, C. Jin, Y. Long, *Phys. Rev. Lett.* **2015**, *115*, 8 087601.

[91] J. M. Perez-Mato, S. V. Gallego, L. Elcoro, E. Tasci, M. I. Aroyo, *J. Phys.: Condens. Matter* **2016**, *28*, 28 286001.

[92] M. S. Senn, N. C. Bristowe, *Acta Crystallogr. A: Foundations and Advances* **2018**, *74*, 4 308.

[93] M. V. Talanov, *Acta Crystallogr. A: Foundations and Advances* **2019**, *75*, 2 379.

[94] J. S. Feng, H. J. Xiang, *Phys. Rev. B* **2016**, *93*, 17 174416.

[95] S. Lv, H. Li, X. Liu, J. Meng, *J. Appl. Phys.* **2011**, *110*, 2 023711.

[96] J. S. Feng, K. Xu, L. Bellaiche, H. J. Xiang, *New J. Phys.* **2018**, *20*, 5 053025.

[97] T. Bayaraa, C. Xu, Y. Yang, H. Xiang, L. Bellaiche, *Phys. Rev. Lett.* **2020**, *125* 067602.

[98] Y. Yang, H. Xiang, H. Zhao, A. Stroppa, J. Zhang, S. Cao, J. Íñiguez, L. Bellaiche, W. Ren, *Phys. Rev. B* **2017**, *96* 104431.

[99] H. Y. Zhou, H. J. Zhao, W. Q. Zhang, X. M. Chen, *Appl. Phys. Lett.* **2015**, *106*, 15 152901.

[100] D. Rahmedov, D. Wang, J. Íñiguez, L. Bellaiche, *Phys. Rev. Lett.* **2012**, *109* 037207.

[101] S. R. Burns, D. Sando, B. Xu, B. Dupé, L. Russell, G. Deng, R. Clements, O. H. C. Paull, J. Seidel, L. Bellaiche, N. Valanoor, C. Ulrich, *npj Quantum Materials* **2019**, *4*, 1 18.

[102] C. Xu, B. Xu, B. Dupé, L. Bellaiche, *Phys. Rev. B* **2019**, *99*, 10 104420.

[103] B. Xu, B. Dupé, C. Xu, H. Xiang, L. Bellaiche, *Phys. Rev. B* **2018**, *98*, 18 84420.

[104] S. Bhattacharjee, D. Rahmedov, D. Wang, J. Íñiguez, L. Bellaiche, *Phys. Rev. Lett.* **2014**, *112*, 14 147601.

[105] L. Chen, C. Xu, H. Tian, H. Xiang, J. Íñiguez, Y. Yang, L. Bellaiche, *Phys. Rev. Lett.* **2019**, *122*, 24 247701.

[106] C. Xu, P. Chen, H. Tan, Y. Yang, H. Xiang, L. Bellaiche, *Phys. Rev. Lett.* **2020**, *125*, 3 037203.

[107] I. I. Naumov, L. Bellaiche, H. Fu, *Nature* **2004**, *432*, 7018 737.

[108] B.-K. Lai, I. Ponomareva, I. I. Naumov, I. Kornev, H. Fu, L. Bellaiche, G. J. Salamo, *Phys. Rev. Lett.* **2006**, *96*, 13 137602.

[109] D. Sichuga, L. Bellaiche, *Phys. Rev. Lett.* **2011**, *106*, 19 196102.

[110] L. Lu, Y. Nahas, M. Liu, H. Du, Z. Jiang, S. Ren, D. Wang, L. Jin, S. Prokhorenko, C.-L. Jia, L. Bellaiche, *Phys. Rev. Lett.* **2018**, *120*, 17 177601.

[111] Y. Nahas, S. Prokhorenko, L. Louis, Z. Gui, I. Kornev, L. Bellaiche, *Nat. Commun.* **2015**, *6*, 1 8542.

[112] M. Gonçalves, C. Escorihuela-Sayalero, P. García-Fernández, J. Junquera, J. Íñiguez, *Sci. Adv.* **2019**, *5* eaau7023.

[113] C.-L. Jia, K. W. Urban, M. Alexe, D. Hesse, I. Vrejoiu, *Science* **2011**, *331*, 6023 1420.

[114] C. T. Nelson, B. Winchester, Y. Zhang, S.-J. Kim, A. Melville, C. Adamo, C. M. Folkman, S.-H. Baek, C.-B. Eom, D. G. Schlom, L.-Q. Chen, X. Pan, *Nano Lett.* **2011**, *11*, 2 828.

[115] A. K. Yadav, C. T. Nelson, S. L. Hsu, Z. Hong, J. D. Clarkson, C. M. Schlepütz, A. R. Damodaran, P. Shafer, E. Arenholz, L. R. Dedon, D. Chen, A. Vishwanath, A. M. Minor, L. Q. Chen, J. F. Scott, L. W. Martin, R. Ramesh, *Nature* **2016**, *530*, 7589 198.

[116] S. Das, Y. L. Tang, Z. Hong, M. A. P. Gonçalves, M. R. McCarter, C. Klewe, K. X. Nguyen, F. Gómez-Ortiz, P. Shafer, E. Arenholz, V. A. Stoica, S.-L. Hsu, B. Wang, C. Ophus, J. F. Liu, C. T. Nelson, S. Saremi, B. Prasad, A. B. Mei, D. G. Schlom, J. Íñiguez, P. García-Fernández, D. A. Muller, L. Q. Chen, J. Junquera, L. W. Martin, R. Ramesh, *Nature* **2019**, *568*, 7752 368.

[117] S. Prosandeev, A. Malashevich, Z. Gui, L. Louis, R. Walter, I. Souza, L. Bellaiche, *Phys. Rev. B* **2013**, *87*, 19 95111.

[118] R. Walter, S. Prokhorenko, Z. Gui, Y. Nahas, L. Bellaiche, *Adv. Electron. Mater.* **2015**, *2*, 1 1500218.

[119] D. Sichuga, W. Ren, S. Prosandeev, L. Bellaiche, *Phys. Rev. Lett.* **2010**, *104*, 20 207603.

[120] W. Ren, L. Bellaiche, *Phys. Rev. Lett.* **2011**, *107*, 12 127202.

[121] K. A. Müller, H. Burkard, *Phys. Rev. B* **1979**, *19*, 7 3593.

[122] S. Prosandeev, A. R. Akbarzadeh, L. Bellaiche, *Phys. Rev. Lett.* **2009**, *102*, 25 257601.

[123] S. Prosandeev, A. Malashevich, I. P. Raevski, L. Bellaiche, *Phys. Rev. B* **2015**, *91*, 10 100101(R).

[124] S. A. F. andO. E. Bochkov, *JETP Lett.* **1981**, *33* 34.

[125] S. A. Flerova, O. E. Bochkov, *Sov. Phys. Crystallogr.* **1982**, *27*, 1 198.

[126] S. A. Popov, N. A. Tikhomirova, S. A. Flerova, *Sov. Phys. Crystallogr.* **1985**, *30*, 3 608.

[127] O. L. Orlov, S. A. Popov, S. A. Flerova, I. L. Tsinman, *Sov. Tech. Phys. Lett.* **1988**, *14*, 2 118.

[128] S. A. Flerova, I. E. Chupis, *Acad.Sci.: Phys.* **1993**, *57*, 3 20.

[129] C. Paillard, R. Mondal, M. Berritta, B. Dkhil, S. Singh, P. M. Oppeneer, L. Bellaiche, In H.-J. Drouhin, J.-E. Wegrowe, M. Razeghi, editors, *Spintronics IX*. SPIE, **2016** 99312E.

[130] R. Mondal, M. Berritta, C. Paillard, S. Singh, B. Dkhil, P. M. Oppeneer, L. Bellaiche, *Phys. Rev. B* **2015**, *92*, 10 100402(R).

[131] L. Bellaiche, W. Ren, S. Singh, *Phys. Rev. B* **2013**, *88*, 16 161102(R).

[132] E. Hall, *Philos. Mag. J. Sci.* **1881**, *12*, 74 157.

[133] N. Nagaosa, J. Sinova, S. Onoda, A. H. MacDonald, N. P. Ong, *Rev. Mod. Phys.* **2010**, *82*, 2 1539.

[134] R. Walter, M. Viret, S. Singh, L. Bellaiche, *J. Phys.: Condens. Matter* **2014**, *26*, 43 432201.

[135] L. L. Campbell, *Nature* **1924**, *113*, 2847 743.

[136] S. Bhattacharjee, S. Singh, D. Wang, M. Viret, L. Bellaiche, *J. Phys.: Condens. Matter* **2014**, *26*, 31 315008.

[137] V. Edelstein, *Solid State Commun.* **1990**, *73*, 3 233.

[138] J. C. R. Sánchez, L. Vila, G. Desfonds, S. Gambarelli, J. P. Attané, J. M. D. Teresa, C. Magén, A. Fert, *Nat. Commun.* **2013**, *4*, 1 2944.

[139] J. P. van der Ziel, P. S. Pershan, L. D. Malmstrom, *Phys. Rev. Lett.* **1965**, *15*, 5 190.

[140] M. Battiato, G. Barbalinardo, P. M. Oppeneer, *Phys. Rev. B* **2014**, *89*, 1 014413.

[141] A. Kirilyuk, A. V. Kimel, T. Rasing, *Rev. Mod. Phys.* **2010**, *82*, 3 2731.

[142] A. V. Kimel, A. Kirilyuk, P. A. Usachev, R. V. Pisarev, A. M. Balbashov, T. Rasing, *Nature* **2005**, *435*, 7042 655.

[143] C. Paillard, R. Walter, S. Singh, B. Dkhil, L. Bellaiche, *J. Phys.: Condens. Matter* **2017**, *29*, 25 254001.

[144] A. Manchon, S. Zhang, *Phys. Rev. B* **2009**, *79*, 9 094422.

[145] B. Hillebrands, A. Thiaville, editors, *Spin Dynamics in Confined Magnetic Structures III*, Springer Berlin Heidelberg, **2006**.

[146] D. Ralph, M. Stiles, *J. Magn. Magn. Mater.* **2008**, *320*, 7 1190.

[147] N. Locatelli, V. Cros, J. Grollier, *Nat. Mater.* **2013**, *13*, 1 11.

[148] E. A. Eliseev, A. N. Morozovska, Y. Gu, A. Y. Borisevich, L.-Q. Chen, V. Gopalan, S. V. Kalinin, *Phys. Rev. B* **2012**, *86* 085416.

[149] A. N. Morozovska, E. A. Eliseev, M. D. Glinchuk, L.-Q. Chen, V. Gopalan, *Phys. Rev. B* **2012**, *85* 094107.

[150] R. K. Vasudevan, W. Wu, J. R. Guest, A. P. Baddorf, A. N. Morozovska, E. A. Eliseev, N. Balke, V. Nagarajan, P. Maksymovych, S. V. Kalinin, *Advanced Functional Materials* **2013**, *23*, 20 2592.

[151] A. Schiaffino, M. Stengel, *Phys. Rev. Lett.* **2017**, *119* 137601.

[152] M. Stengel, private communication.

[153] K. Momma, F. Izumi, *J. Appl. Crystal.* **2011**, *44*, 6 1272.

[154] W. R. Inc., Mathematica, Version 12.0, URL `https://www.wolfram.com/mathematica`, Champaign, IL, 2019.

Table 1: Transformation rules for various order parameters in ABX_3 perovskites. The order parameters of tiltings (for the BX_6 octahedra), displacement and magnetism are represented by ω, u, and m, respectively. Also, we adopt the convention that the symmetry operators are centered on the A site. FE, AFE, FM and AFM wordings denote that the corresponding order parameters belong to the ferroelectric, anti-ferroelectric, ferromagnetic, and anti-ferromagnetic categories. Some order parameters and their transformation rules have already been proposed in, *e.g.*, Ref.[26].

	2_{001}	2_{010}	3^+_{111}	2_{110}	$\bar{1}$	$1'$	
ω_x^R	$-\omega_x^R$	$-\omega_x^R$	ω_y^R	$-\omega_y^R$	$-\omega_x^R$	ω_x^R	
ω_y^R	$-\omega_y^R$	ω_y^R	ω_z^R	$-\omega_x^R$	$-\omega_y^R$	ω_y^R	Tiltings (R point)
ω_z^R	ω_z^R	$-\omega_z^R$	ω_x^R	ω_z^R	$-\omega_z^R$	ω_z^R	
ω_x^{Mx}	ω_x^{Mx}	ω_x^{Mx}	ω_y^{My}	$-\omega_y^{My}$	ω_x^{Mx}	ω_x^{Mx}	
ω_y^{My}	ω_y^{My}	ω_y^{My}	ω_z^{Mz}	$-\omega_x^{Mx}$	ω_y^{My}	ω_y^{My}	Tiltings (M point)
ω_z^{Mz}	ω_z^{Mz}	ω_z^{Mz}	ω_x^{Mx}	$-\omega_z^{Mz}$	ω_z^{Mz}	ω_z^{Mz}	
$u_{B,x}^R$	$-u_{B,x}^R$	$-u_{B,x}^R$	$u_{B,y}^R$	$-u_{B,y}^R$	$u_{B,x}^R$	$u_{B,x}^R$	(B site)
$u_{B,y}^R$	$-u_{B,y}^R$	$u_{B,y}^R$	$u_{B,z}^R$	$-u_{B,x}^R$	$u_{B,y}^R$	$u_{B,y}^R$	AFE (R point)
$u_{B,z}^R$	$u_{B,z}^R$	$-u_{B,z}^R$	$u_{B,x}^R$	$u_{B,z}^R$	$u_{B,z}^R$	$u_{B,z}^R$	
$u_{B,x}^\Gamma$	$-u_{B,x}^\Gamma$	$-u_{B,x}^\Gamma$	$u_{B,y}^\Gamma$	$u_{B,y}^\Gamma$	$-u_{B,x}^\Gamma$	$u_{B,x}^\Gamma$	(B site)
$u_{B,y}^\Gamma$	$-u_{B,y}^\Gamma$	$u_{B,y}^\Gamma$	$u_{B,z}^\Gamma$	$u_{B,x}^\Gamma$	$-u_{B,y}^\Gamma$	$u_{B,y}^\Gamma$	FE (Γ point)
$u_{B,z}^\Gamma$	$u_{B,z}^\Gamma$	$-u_{B,z}^\Gamma$	$u_{B,x}^\Gamma$	$-u_{B,z}^\Gamma$	$-u_{B,z}^\Gamma$	$u_{B,z}^\Gamma$	
$u_{B,x}^{Xx}$	$u_{B,x}^{Xx}$	$u_{B,x}^{Xx}$	$u_{B,y}^{Xy}$	$u_{B,y}^{Xy}$	$u_{B,x}^{Xx}$	$u_{B,x}^{Xx}$	
$u_{B,y}^{Xx}$	$u_{B,y}^{Xx}$	$-u_{B,y}^{Xx}$	$u_{B,z}^{Xy}$	$u_{B,x}^{Xy}$	$u_{B,y}^{Xx}$	$u_{B,y}^{Xx}$	
$u_{B,z}^{Xx}$	$-u_{B,z}^{Xx}$	$u_{B,z}^{Xx}$	$u_{B,x}^{Xy}$	$-u_{B,z}^{Xy}$	$u_{B,z}^{Xx}$	$u_{B,z}^{Xx}$	
$u_{B,x}^{Xy}$	$u_{B,x}^{Xy}$	$-u_{B,x}^{Xy}$	$u_{B,y}^{Xz}$	$u_{B,y}^{Xx}$	$u_{B,x}^{Xy}$	$u_{B,x}^{Xy}$	(B site)
$u_{B,y}^{Xy}$	$u_{B,y}^{Xy}$	$u_{B,y}^{Xy}$	$u_{B,z}^{Xz}$	$u_{B,x}^{Xx}$	$u_{B,y}^{Xy}$	$u_{B,y}^{Xy}$	AFE (X point)
$u_{B,z}^{Xy}$	$-u_{B,z}^{Xy}$	$-u_{B,z}^{Xy}$	$u_{B,x}^{Xz}$	$-u_{B,z}^{Xx}$	$u_{B,z}^{Xy}$	$u_{B,z}^{Xy}$	
$u_{B,x}^{Xz}$	$-u_{B,x}^{Xz}$	$u_{B,x}^{Xz}$	$u_{B,y}^{Xx}$	$-u_{B,y}^{Xz}$	$u_{B,x}^{Xz}$	$u_{B,x}^{Xz}$	
$u_{B,y}^{Xz}$	$-u_{B,y}^{Xz}$	$-u_{B,y}^{Xz}$	$u_{B,z}^{Xx}$	$-u_{B,x}^{Xz}$	$u_{B,y}^{Xz}$	$u_{B,y}^{Xz}$	
$u_{B,z}^{Xz}$	$u_{B,z}^{Xz}$	$u_{B,z}^{Xz}$	$u_{B,x}^{Xx}$	$u_{B,z}^{Xz}$	$u_{B,z}^{Xz}$	$u_{B,z}^{Xz}$	
$u_{B,x}^{Mx}$	$u_{B,x}^{Mx}$	$u_{B,x}^{Mx}$	$u_{B,y}^{My}$	$-u_{B,y}^{My}$	$-u_{B,x}^{Mx}$	$u_{B,x}^{Mx}$	
$u_{B,y}^{Mx}$	$u_{B,y}^{Mx}$	$-u_{B,y}^{Mx}$	$u_{B,z}^{My}$	$-u_{B,x}^{My}$	$-u_{B,y}^{Mx}$	$u_{B,y}^{Mx}$	
$u_{B,z}^{Mx}$	$-u_{B,z}^{Mx}$	$u_{B,z}^{Mx}$	$u_{B,x}^{My}$	$u_{B,z}^{My}$	$-u_{B,z}^{Mx}$	$u_{B,z}^{Mx}$	
$u_{B,x}^{My}$	$u_{B,x}^{My}$	$-u_{B,x}^{My}$	$u_{B,y}^{Mz}$	$-u_{B,y}^{Mx}$	$-u_{B,x}^{My}$	$u_{B,x}^{My}$	(B site)
$u_{B,y}^{My}$	$u_{B,y}^{My}$	$u_{B,y}^{My}$	$u_{B,z}^{Mz}$	$-u_{B,x}^{Mx}$	$-u_{B,y}^{My}$	$u_{B,y}^{My}$	AFE (M point)
$u_{B,z}^{My}$	$-u_{B,z}^{My}$	$-u_{B,z}^{My}$	$u_{B,x}^{Mz}$	$u_{B,z}^{Mx}$	$-u_{B,z}^{My}$	$u_{B,z}^{My}$	
$u_{B,x}^{Mz}$	$-u_{B,x}^{Mz}$	$u_{B,x}^{Mz}$	$u_{B,y}^{Mx}$	$u_{B,y}^{Mz}$	$-u_{B,x}^{Mz}$	$u_{B,x}^{Mz}$	
$u_{B,y}^{Mz}$	$-u_{B,y}^{Mz}$	$-u_{B,y}^{Mz}$	$u_{B,z}^{Mx}$	$u_{B,x}^{Mz}$	$-u_{B,y}^{Mz}$	$u_{B,y}^{Mz}$	
$u_{B,z}^{Mz}$	$u_{B,z}^{Mz}$	$u_{B,z}^{Mz}$	$u_{B,x}^{Mx}$	$-u_{B,z}^{Mz}$	$-u_{B,z}^{Mz}$	$u_{B,z}^{Mz}$	
$u_{A,x}^R$	$-u_{A,x}^R$	$-u_{A,x}^R$	$u_{A,y}^R$	$u_{A,y}^R$	$-u_{A,x}^R$	$u_{A,x}^R$	(A site)
$u_{A,y}^R$	$-u_{A,y}^R$	$u_{A,y}^R$	$u_{A,z}^R$	$u_{A,x}^R$	$-u_{A,y}^R$	$u_{A,y}^R$	AFE (R point)
$u_{A,z}^R$	$u_{A,z}^R$	$-u_{A,z}^R$	$u_{A,x}^R$	$-u_{A,z}^R$	$-u_{A,z}^R$	$u_{A,z}^R$	
$u_{A,x}^\Gamma$	$-u_{A,x}^\Gamma$	$-u_{A,x}^\Gamma$	$u_{A,y}^\Gamma$	$u_{A,y}^\Gamma$	$-u_{A,x}^\Gamma$	$u_{A,x}^\Gamma$	(A site)
$u_{A,y}^\Gamma$	$-u_{A,y}^\Gamma$	$u_{A,y}^\Gamma$	$u_{A,z}^\Gamma$	$u_{A,x}^\Gamma$	$-u_{A,y}^\Gamma$	$u_{A,y}^\Gamma$	FE (Γ point)
$u_{A,z}^\Gamma$	$u_{A,z}^\Gamma$	$-u_{A,z}^\Gamma$	$u_{A,x}^\Gamma$	$-u_{A,z}^\Gamma$	$-u_{A,z}^\Gamma$	$u_{A,z}^\Gamma$	
$u_{A,x}^{Xx}$	$-u_{A,x}^{Xx}$	$-u_{A,x}^{Xx}$	$u_{A,y}^{Xy}$	$u_{A,y}^{Xy}$	$-u_{A,x}^{Xx}$	$u_{A,x}^{Xx}$	
$u_{A,y}^{Xx}$	$-u_{A,y}^{Xx}$	$u_{A,y}^{Xx}$	$u_{A,z}^{Xy}$	$u_{A,x}^{Xy}$	$-u_{A,y}^{Xx}$	$u_{A,y}^{Xx}$	
$u_{A,z}^{Xx}$	$u_{A,z}^{Xx}$	$-u_{A,z}^{Xx}$	$u_{A,x}^{Xy}$	$-u_{A,z}^{Xy}$	$-u_{A,z}^{Xx}$	$u_{A,z}^{Xx}$	
$u_{A,x}^{Xy}$	$-u_{A,x}^{Xy}$	$-u_{A,x}^{Xy}$	$u_{A,y}^{Xz}$	$u_{A,y}^{Xx}$	$-u_{A,x}^{Xy}$	$u_{A,x}^{Xy}$	(A site)
$u_{A,y}^{Xy}$	$-u_{A,y}^{Xy}$	$u_{A,y}^{Xy}$	$u_{A,z}^{Xz}$	$u_{A,x}^{Xx}$	$-u_{A,y}^{Xy}$	$u_{A,y}^{Xy}$	AFE (X point)
$u_{A,z}^{Xy}$	$u_{A,z}^{Xy}$	$-u_{A,z}^{Xy}$	$u_{A,x}^{Xz}$	$-u_{A,z}^{Xx}$	$-u_{A,z}^{Xy}$	$u_{A,z}^{Xy}$	

$u^{Xz}_{A,x}$	$-u^{Xz}_{A,x}$	$-u^{Xz}_{A,x}$	$u^{Xx}_{A,y}$	$u^{Xz}_{A,y}$	$-u^{Xz}_{A,x}$	$u^{Xz}_{A,x}$	
$u^{Xz}_{A,y}$	$-u^{Xz}_{A,y}$	$u^{Xz}_{A,y}$	$u^{Xx}_{A,z}$	$u^{Xz}_{A,x}$	$-u^{Xz}_{A,y}$	$u^{Xz}_{A,y}$	
$u^{Xz}_{A,z}$	$u^{Xz}_{A,z}$	$-u^{Xz}_{A,z}$	$u^{Xx}_{A,x}$	$-u^{Xz}_{A,z}$	$-u^{Xz}_{A,z}$	$u^{Xz}_{A,z}$	
$u^{Mx}_{A,x}$	$-u^{Mx}_{A,x}$	$-u^{Mx}_{A,x}$	$u^{My}_{A,y}$	$u^{My}_{A,y}$	$-u^{Mx}_{A,x}$	$u^{Mx}_{A,x}$	
$u^{Mx}_{A,y}$	$-u^{Mx}_{A,y}$	$u^{Mx}_{A,y}$	$u^{My}_{A,z}$	$u^{My}_{A,x}$	$-u^{Mx}_{A,y}$	$u^{Mx}_{A,y}$	
$u^{Mx}_{A,z}$	$u^{Mx}_{A,z}$	$-u^{Mx}_{A,z}$	$u^{My}_{A,x}$	$-u^{My}_{A,z}$	$-u^{Mx}_{A,z}$	$u^{Mx}_{A,z}$	
$u^{My}_{A,x}$	$-u^{My}_{A,x}$	$-u^{My}_{A,x}$	$u^{Mz}_{A,y}$	$u^{Mx}_{A,y}$	$-u^{My}_{A,x}$	$u^{My}_{A,x}$	(A site)
$u^{My}_{A,y}$	$-u^{My}_{A,y}$	$u^{My}_{A,y}$	$u^{Mz}_{A,z}$	$u^{Mx}_{A,x}$	$-u^{My}_{A,y}$	$u^{My}_{A,y}$	AFE (M point)
$u^{My}_{A,z}$	$u^{My}_{A,z}$	$-u^{My}_{A,z}$	$u^{Mz}_{A,x}$	$-u^{Mx}_{A,z}$	$-u^{My}_{A,z}$	$u^{My}_{A,z}$	
$u^{Mz}_{A,x}$	$-u^{Mz}_{A,x}$	$-u^{Mz}_{A,x}$	$u^{Mx}_{A,y}$	$u^{Mz}_{A,y}$	$-u^{Mz}_{A,x}$	$u^{Mz}_{A,x}$	
$u^{Mz}_{A,y}$	$-u^{Mz}_{A,y}$	$u^{Mz}_{A,y}$	$u^{Mx}_{A,z}$	$u^{Mz}_{A,x}$	$-u^{Mz}_{A,y}$	$u^{Mz}_{A,y}$	
$u^{Mz}_{A,z}$	$u^{Mz}_{A,z}$	$-u^{Mz}_{A,z}$	$u^{Mx}_{A,x}$	$-u^{Mz}_{A,z}$	$-u^{Mz}_{A,z}$	$u^{Mz}_{A,z}$	
$m^{R}_{B,x}$	$-m^{R}_{B,x}$	$-m^{R}_{B,x}$	$m^{R}_{B,y}$	$-m^{R}_{B,y}$	$-m^{R}_{B,x}$	$-m^{R}_{B,x}$	(B site)
$m^{R}_{B,y}$	$-m^{R}_{B,y}$	$m^{R}_{B,y}$	$m^{R}_{B,z}$	$-m^{R}_{B,x}$	$-m^{R}_{B,y}$	$-m^{R}_{B,y}$	AFM (R point)
$m^{R}_{B,z}$	$m^{R}_{B,z}$	$-m^{R}_{B,z}$	$m^{R}_{B,x}$	$m^{R}_{B,z}$	$-m^{R}_{B,z}$	$-m^{R}_{B,z}$	
$m^{\Gamma}_{B,x}$	$-m^{\Gamma}_{B,x}$	$-m^{\Gamma}_{B,x}$	$m^{\Gamma}_{B,y}$	$m^{\Gamma}_{B,y}$	$m^{\Gamma}_{B,x}$	$-m^{\Gamma}_{B,x}$	(B site)
$m^{\Gamma}_{B,y}$	$-m^{\Gamma}_{B,y}$	$m^{\Gamma}_{B,y}$	$m^{\Gamma}_{B,z}$	$m^{\Gamma}_{B,x}$	$m^{\Gamma}_{B,y}$	$-m^{\Gamma}_{B,y}$	FM (Γ point)
$m^{\Gamma}_{B,z}$	$m^{\Gamma}_{B,z}$	$-m^{\Gamma}_{B,z}$	$m^{\Gamma}_{B,x}$	$-m^{\Gamma}_{B,z}$	$m^{\Gamma}_{B,z}$	$-m^{\Gamma}_{B,z}$	
$m^{Xx}_{B,x}$	$m^{Xx}_{B,x}$	$m^{Xx}_{B,x}$	$m^{Xy}_{B,y}$	$m^{Xy}_{B,y}$	$-m^{Xx}_{B,x}$	$-m^{Xx}_{B,x}$	
$m^{Xx}_{B,y}$	$m^{Xx}_{B,y}$	$-m^{Xx}_{B,y}$	$m^{Xy}_{B,z}$	$m^{Xy}_{B,x}$	$-m^{Xx}_{B,y}$	$-m^{Xx}_{B,y}$	
$m^{Xx}_{B,z}$	$-m^{Xx}_{B,z}$	$m^{Xx}_{B,z}$	$m^{Xy}_{B,x}$	$-m^{Xy}_{B,z}$	$-m^{Xx}_{B,z}$	$-m^{Xx}_{B,z}$	
$m^{Xy}_{B,x}$	$m^{Xy}_{B,x}$	$-m^{Xy}_{B,x}$	$m^{Xz}_{B,y}$	$m^{Xx}_{B,y}$	$-m^{Xy}_{B,x}$	$-m^{Xy}_{B,x}$	(B site)
$m^{Xy}_{B,y}$	$m^{Xy}_{B,y}$	$m^{Xy}_{B,y}$	$m^{Xz}_{B,z}$	$m^{Xx}_{B,x}$	$-m^{Xy}_{B,y}$	$-m^{Xy}_{B,y}$	AFM (X point)
$m^{Xy}_{B,z}$	$-m^{Xy}_{B,z}$	$-m^{Xy}_{B,z}$	$m^{Xz}_{B,x}$	$-m^{Xx}_{B,z}$	$-m^{Xy}_{B,z}$	$-m^{Xy}_{B,z}$	
$m^{Xz}_{B,x}$	$-m^{Xz}_{B,x}$	$m^{Xz}_{B,x}$	$m^{Xx}_{B,y}$	$-m^{Xz}_{B,y}$	$-m^{Xz}_{B,x}$	$-m^{Xz}_{B,x}$	
$m^{Xz}_{B,y}$	$-m^{Xz}_{B,y}$	$-m^{Xz}_{B,y}$	$m^{Xx}_{B,z}$	$-m^{Xz}_{B,x}$	$-m^{Xz}_{B,y}$	$-m^{Xz}_{B,y}$	
$m^{Xz}_{B,z}$	$m^{Xz}_{B,z}$	$m^{Xz}_{B,z}$	$m^{Xx}_{B,x}$	$m^{Xz}_{B,z}$	$-m^{Xz}_{B,z}$	$-m^{Xz}_{B,z}$	
$m^{Mx}_{B,x}$	$m^{Mx}_{B,x}$	$m^{Mx}_{B,x}$	$m^{My}_{B,y}$	$-m^{My}_{B,y}$	$m^{Mx}_{B,x}$	$-m^{Mx}_{B,x}$	
$m^{Mx}_{B,y}$	$m^{Mx}_{B,y}$	$-m^{Mx}_{B,y}$	$m^{My}_{B,z}$	$-m^{My}_{B,x}$	$m^{Mx}_{B,y}$	$-m^{Mx}_{B,y}$	
$m^{Mx}_{B,z}$	$-m^{Mx}_{B,z}$	$m^{Mx}_{B,z}$	$m^{My}_{B,x}$	$m^{My}_{B,z}$	$m^{Mx}_{B,z}$	$-m^{Mx}_{B,z}$	
$m^{My}_{B,x}$	$m^{My}_{B,x}$	$-m^{My}_{B,x}$	$m^{Mz}_{B,y}$	$-m^{Mx}_{B,y}$	$m^{My}_{B,x}$	$-m^{My}_{B,x}$	(B site)
$m^{My}_{B,y}$	$m^{My}_{B,y}$	$m^{My}_{B,y}$	$m^{Mz}_{B,z}$	$-m^{Mx}_{B,x}$	$m^{My}_{B,y}$	$-m^{My}_{B,y}$	AFM (M point)
$m^{My}_{B,z}$	$-m^{My}_{B,z}$	$-m^{My}_{B,z}$	$m^{Mz}_{B,x}$	$m^{Mx}_{B,z}$	$m^{My}_{B,z}$	$-m^{My}_{B,z}$	
$m^{Mz}_{B,x}$	$-m^{Mz}_{B,x}$	$m^{Mz}_{B,x}$	$m^{Mx}_{B,y}$	$m^{Mz}_{B,y}$	$m^{Mz}_{B,x}$	$-m^{Mz}_{B,x}$	
$m^{Mz}_{B,y}$	$-m^{Mz}_{B,y}$	$-m^{Mz}_{B,y}$	$m^{Mx}_{B,z}$	$m^{Mz}_{B,x}$	$m^{Mz}_{B,y}$	$-m^{Mz}_{B,y}$	
$m^{Mz}_{B,z}$	$m^{Mz}_{B,z}$	$m^{Mz}_{B,z}$	$m^{Mx}_{B,x}$	$-m^{Mz}_{B,z}$	$m^{Mz}_{B,z}$	$-m^{Mz}_{B,z}$	
$m^{R}_{A,x}$	$-m^{R}_{A,x}$	$-m^{R}_{A,x}$	$m^{R}_{A,y}$	$m^{R}_{A,y}$	$m^{R}_{A,x}$	$-m^{R}_{A,x}$	(A site)
$m^{R}_{A,y}$	$-m^{R}_{A,y}$	$m^{R}_{A,y}$	$m^{R}_{A,z}$	$m^{R}_{A,x}$	$m^{R}_{A,y}$	$-m^{R}_{A,y}$	AFM (R point)
$m^{R}_{A,z}$	$m^{R}_{A,z}$	$-m^{R}_{A,z}$	$m^{R}_{A,x}$	$-m^{R}_{A,z}$	$m^{R}_{A,z}$	$-m^{R}_{A,z}$	
$m^{\Gamma}_{A,x}$	$-m^{\Gamma}_{A,x}$	$-m^{\Gamma}_{A,x}$	$m^{\Gamma}_{A,y}$	$m^{\Gamma}_{A,y}$	$m^{\Gamma}_{A,x}$	$-m^{\Gamma}_{A,x}$	(A site)
$m^{\Gamma}_{A,y}$	$-m^{\Gamma}_{A,y}$	$m^{\Gamma}_{A,y}$	$m^{\Gamma}_{A,z}$	$m^{\Gamma}_{A,x}$	$m^{\Gamma}_{A,y}$	$-m^{\Gamma}_{A,y}$	FM (Γ point)
$m^{\Gamma}_{A,z}$	$m^{\Gamma}_{A,z}$	$-m^{\Gamma}_{A,z}$	$m^{\Gamma}_{A,x}$	$-m^{\Gamma}_{A,z}$	$m^{\Gamma}_{A,z}$	$-m^{\Gamma}_{A,z}$	
$m^{Xx}_{A,x}$	$-m^{Xx}_{A,x}$	$-m^{Xx}_{A,x}$	$m^{Xy}_{A,y}$	$m^{Xy}_{A,y}$	$m^{Xx}_{A,x}$	$-m^{Xx}_{A,x}$	
$m^{Xx}_{A,y}$	$-m^{Xx}_{A,y}$	$m^{Xx}_{A,y}$	$m^{Xy}_{A,z}$	$m^{Xy}_{A,x}$	$m^{Xx}_{A,y}$	$-m^{Xx}_{A,y}$	
$m^{Xx}_{A,z}$	$m^{Xx}_{A,z}$	$-m^{Xx}_{A,z}$	$m^{Xy}_{A,x}$	$-m^{Xy}_{A,z}$	$m^{Xx}_{A,z}$	$-m^{Xx}_{A,z}$	
$m^{Xy}_{A,x}$	$-m^{Xy}_{A,x}$	$-m^{Xy}_{A,x}$	$m^{Xz}_{A,y}$	$m^{Xx}_{A,y}$	$m^{Xy}_{A,x}$	$-m^{Xy}_{A,x}$	(A site)
$m^{Xy}_{A,y}$	$-m^{Xy}_{A,y}$	$m^{Xy}_{A,y}$	$m^{Xz}_{A,z}$	$m^{Xx}_{A,x}$	$m^{Xy}_{A,y}$	$-m^{Xy}_{A,y}$	AFM (X point)

$m^{Xy}_{A,z}$	$m^{Xy}_{A,z}$	$-m^{Xy}_{A,z}$	$m^{Xz}_{A,x}$	$-m^{Xx}_{A,z}$	$m^{Xy}_{A,z}$	$-m^{Xy}_{A,z}$	
$m^{Xz}_{A,x}$	$-m^{Xz}_{A,x}$	$-m^{Xz}_{A,x}$	$m^{Xx}_{A,y}$	$m^{Xz}_{A,y}$	$m^{Xz}_{A,x}$	$-m^{Xz}_{A,x}$	
$m^{Xz}_{A,y}$	$-m^{Xz}_{A,y}$	$m^{Xz}_{A,y}$	$m^{Xx}_{A,z}$	$m^{Xz}_{A,x}$	$m^{Xz}_{A,y}$	$-m^{Xz}_{A,y}$	
$m^{Xz}_{A,z}$	$m^{Xz}_{A,z}$	$-m^{Xz}_{A,z}$	$m^{Xx}_{A,x}$	$-m^{Xz}_{A,z}$	$m^{Xz}_{A,z}$	$-m^{Xz}_{A,z}$	
$m^{Mx}_{A,x}$	$-m^{Mx}_{A,x}$	$-m^{Mx}_{A,x}$	$m^{My}_{A,y}$	$m^{My}_{A,y}$	$m^{Mx}_{A,x}$	$-m^{Mx}_{A,x}$	
$m^{Mx}_{A,y}$	$-m^{Mx}_{A,y}$	$m^{Mx}_{A,y}$	$m^{My}_{A,z}$	$m^{My}_{A,x}$	$m^{Mx}_{A,y}$	$-m^{Mx}_{A,y}$	
$m^{Mx}_{A,z}$	$m^{Mx}_{A,z}$	$-m^{Mx}_{A,z}$	$m^{My}_{A,x}$	$-m^{My}_{A,z}$	$m^{Mx}_{A,z}$	$-m^{Mx}_{A,z}$	
$m^{My}_{A,x}$	$-m^{My}_{A,x}$	$-m^{My}_{A,x}$	$m^{Mz}_{A,y}$	$m^{Mx}_{A,y}$	$m^{My}_{A,x}$	$-m^{My}_{A,x}$	(A site)
$m^{My}_{A,y}$	$-m^{My}_{A,y}$	$m^{My}_{A,y}$	$m^{Mz}_{A,z}$	$m^{Mx}_{A,x}$	$m^{My}_{A,y}$	$-m^{My}_{A,y}$	AFM (M point)
$m^{My}_{A,z}$	$m^{My}_{A,z}$	$-m^{My}_{A,z}$	$m^{Mz}_{A,x}$	$-m^{Mx}_{A,z}$	$m^{My}_{A,z}$	$-m^{My}_{A,z}$	
$m^{Mz}_{A,x}$	$-m^{Mz}_{A,x}$	$-m^{Mz}_{A,x}$	$m^{Mx}_{A,y}$	$m^{Mz}_{A,y}$	$m^{Mz}_{A,x}$	$-m^{Mz}_{A,x}$	
$m^{Mz}_{A,y}$	$-m^{Mz}_{A,y}$	$m^{Mz}_{A,y}$	$m^{Mx}_{A,z}$	$m^{Mz}_{A,x}$	$m^{Mz}_{A,y}$	$-m^{Mz}_{A,y}$	
$m^{Mz}_{A,z}$	$m^{Mz}_{A,z}$	$-m^{Mz}_{A,z}$	$m^{Mx}_{A,x}$	$-m^{Mz}_{A,z}$	$m^{Mz}_{A,z}$	$-m^{Mz}_{A,z}$	
η_{xy}	η_{xy}	$-\eta_{xy}$	η_{yz}	η_{xy}	η_{xy}	η_{xy}	
η_{yz}	$-\eta_{yz}$	$-\eta_{yz}$	η_{zx}	$-\eta_{zx}$	η_{yz}	η_{yz}	
η_{zx}	$-\eta_{zx}$	η_{zx}	η_{xy}	$-\eta_{yz}$	η_{zx}	η_{zx}	Strain
η_{xx}	η_{xx}	η_{xx}	η_{yy}	η_{yy}	η_{xx}	η_{xx}	
η_{yy}	η_{yy}	η_{yy}	η_{zz}	η_{xx}	η_{yy}	η_{yy}	
η_{zz}	η_{zz}	η_{zz}	η_{xx}	η_{zz}	η_{zz}	η_{zz}	

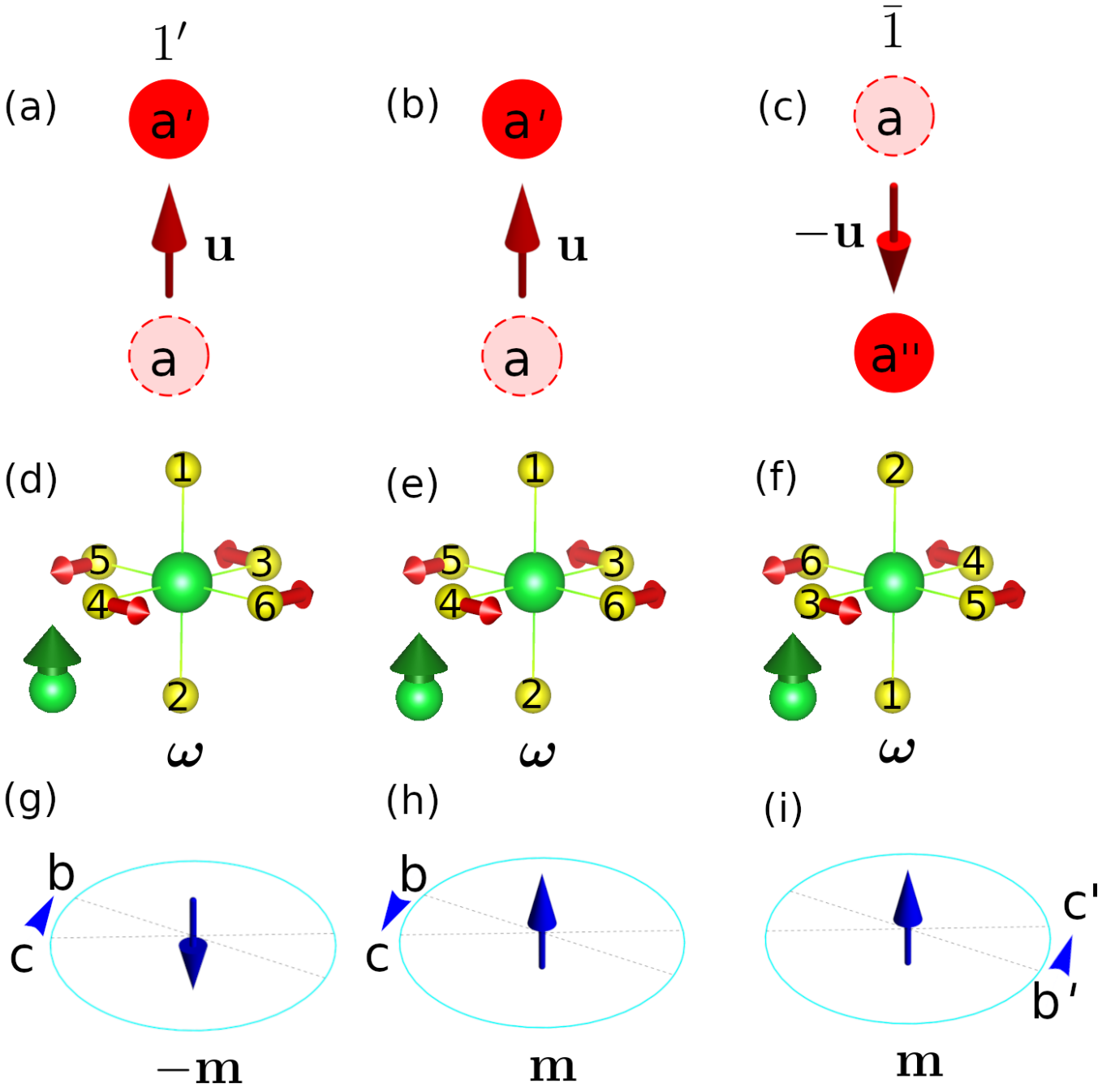

Figure 1: Sketches of displacement (b), rotation of BX_6 octahedra (e) and magnetization (h) vectors, and their transformations under time reversal (a, d, g) and inversion (c, f, i). In panel b, the inversion center locates at the position bisecting "a" and "a′"; in panel e, the inversion is centered at the B ion (green sphere); in panel h, the inversion is the center of the cyan circle.

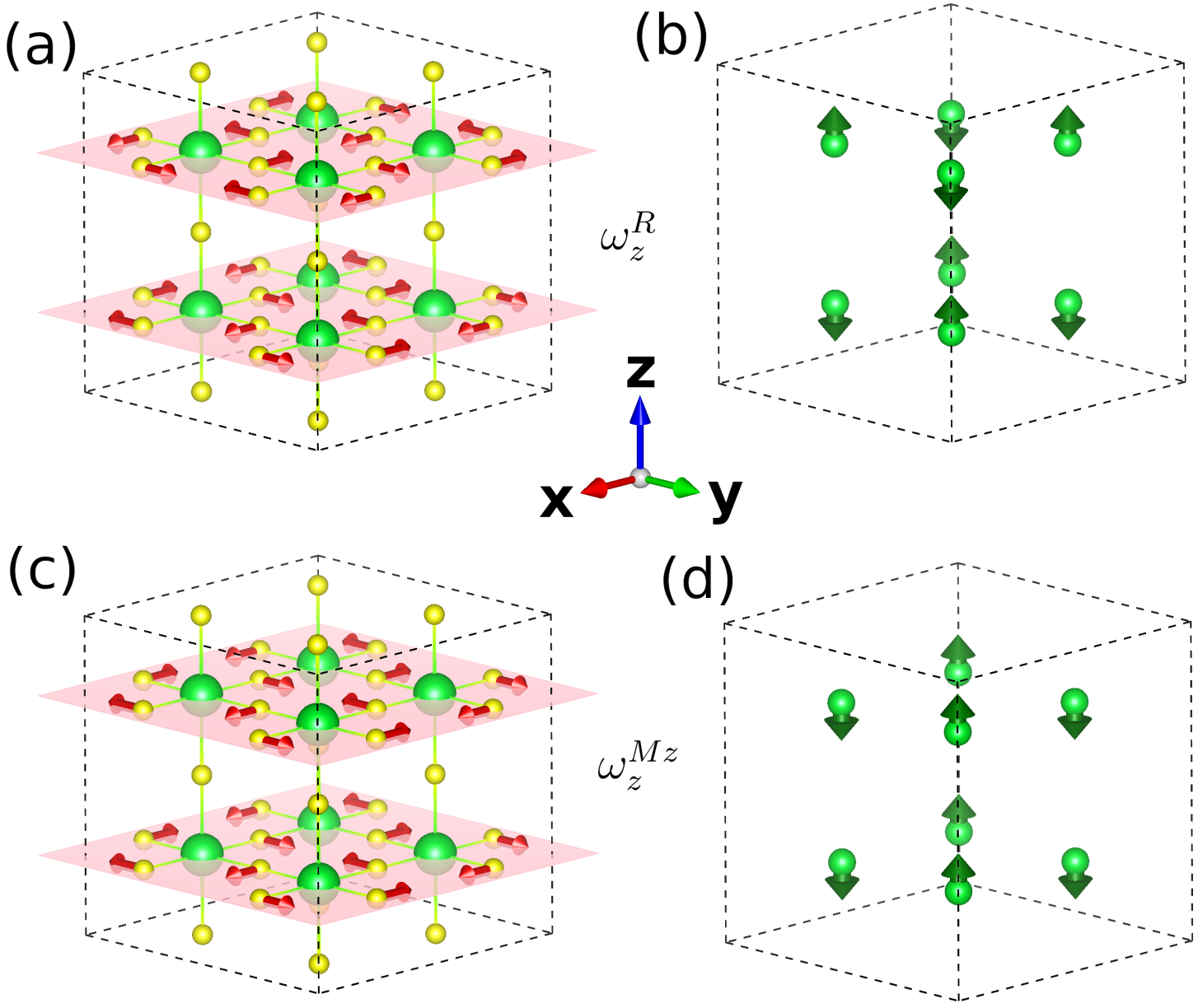

Figure 2: Sketches of anti-phase (a) and in-phase (c) tiltings of BX_6 octahedra about the z direction for ABX_3 perovskites, and their representations by the $\boldsymbol{\omega}$ vectors (b, d). Here, the green and yellow spheres denote the B and X ions, while the A ions are not shown for clarity.

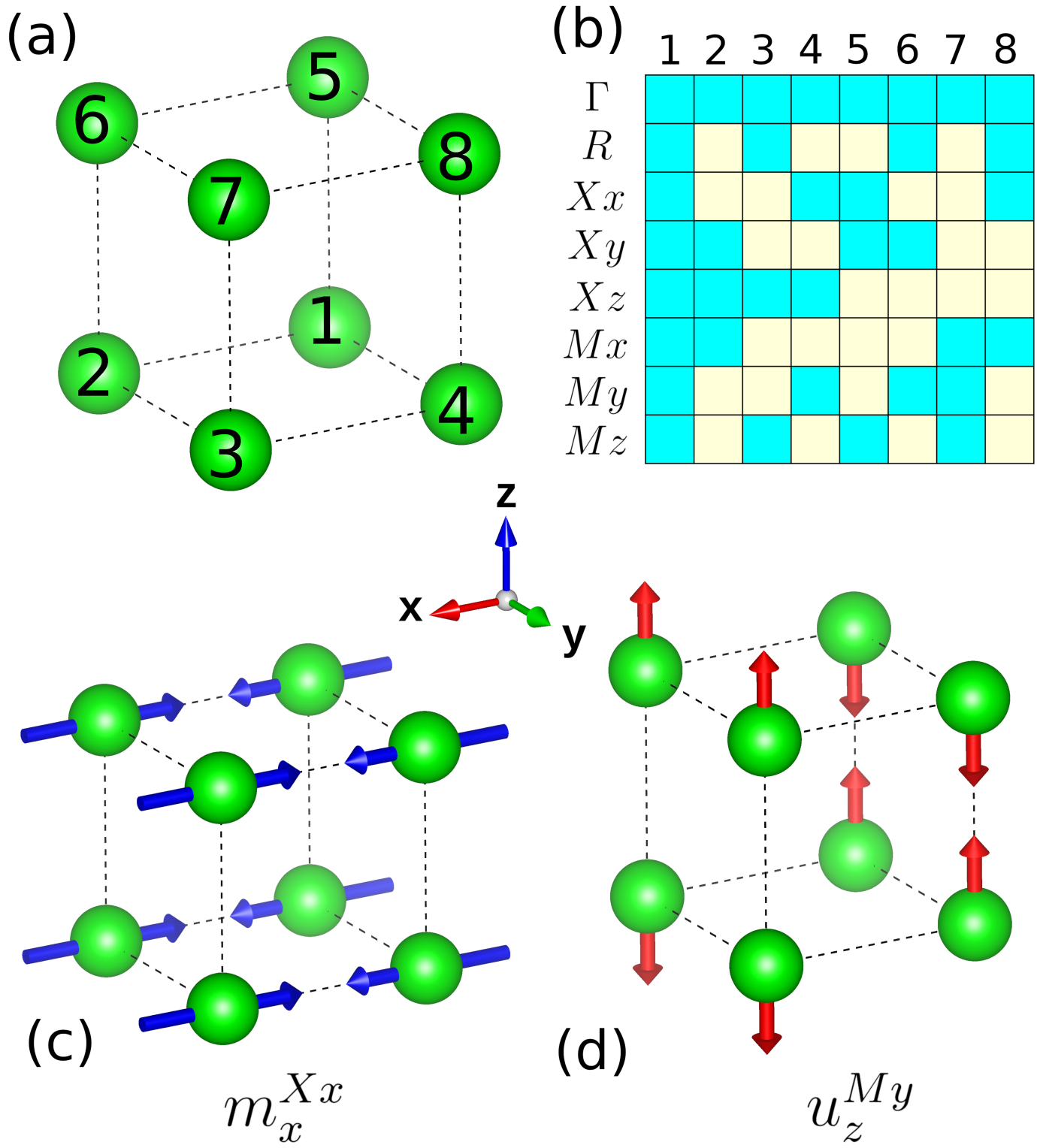

Figure 3: Definition of $q-$points and the modulations. Panel a shows the A or B sublattices in ABX_3 perovskites. Panel b defines the modulations of various $q-$points; the number (1 to 8) denoted the ions labelled by numbers in panel a; the symbols (e.g., Γ, R) mark the $q-$points. Also, in panel b, the cyan and yellow colors indicate that the physical quantities centered on the corresponding ions are with plus and minus signs, respectively. Panels c and d are examples of magnetic structures and structural distortions (see Text); the blue and red arrows are magnetic moments and displacements, respectively.

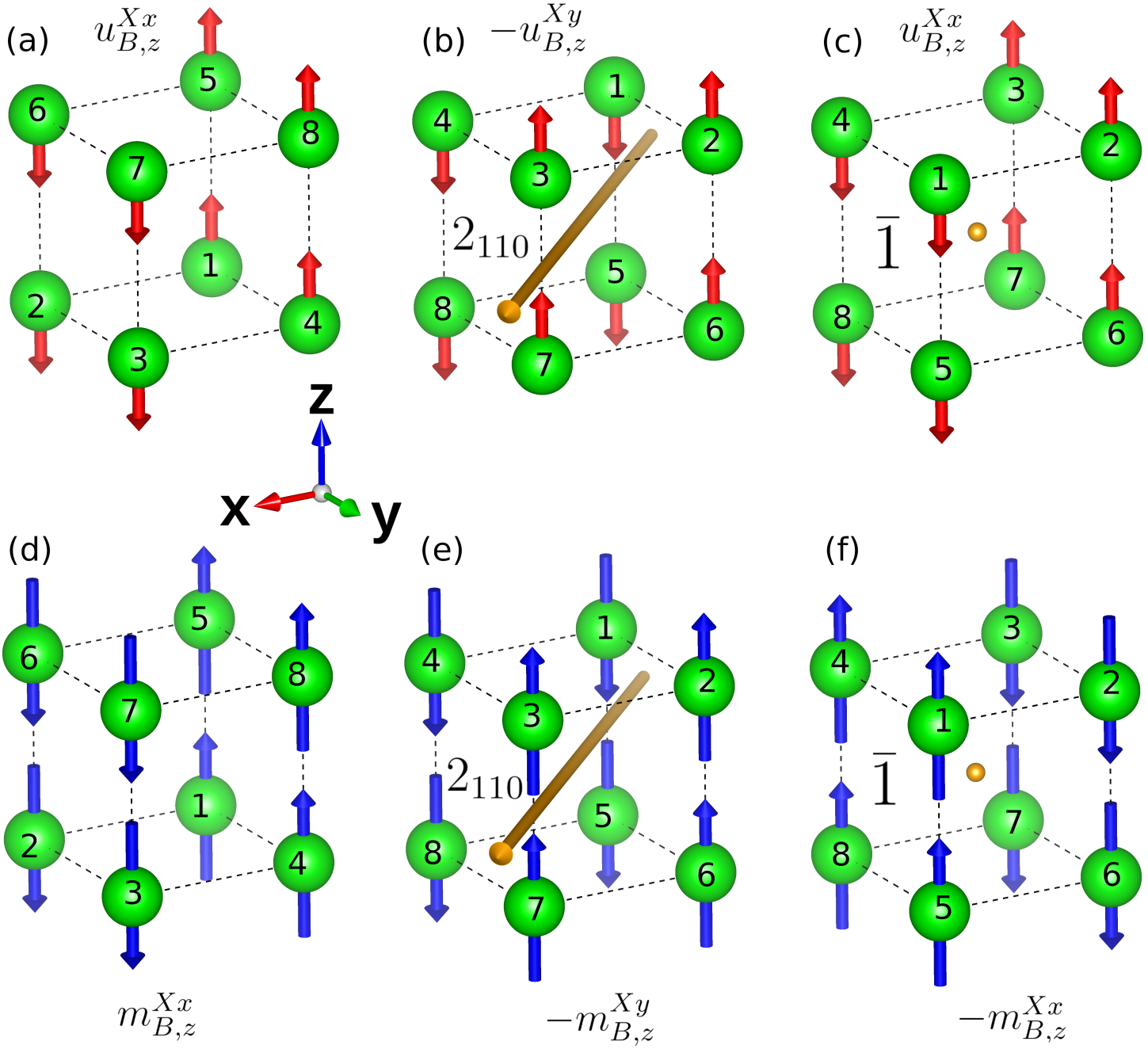

Figure 4: The transformations of order parameters under the rotational operations 2_{110} and inversion $\bar{1}$. Panels a and d are the patterns of $u^{Xx}_{B,z}$ and $m^{Xx}_{B,z}$, respectively. Panels b and e (respectively, c and f) are the transformed patterns by 2_{110} (respectively, by $\bar{1}$). The magnetic moments and displacements are represented by blue and red arrows, respectively. The B ions are shown as green spheres, while the 2_{110} rotational axis and inversion center are denoted by yellow arrow and small yellow sphere (e.g., centered on A ion of ABX_3), respectively.

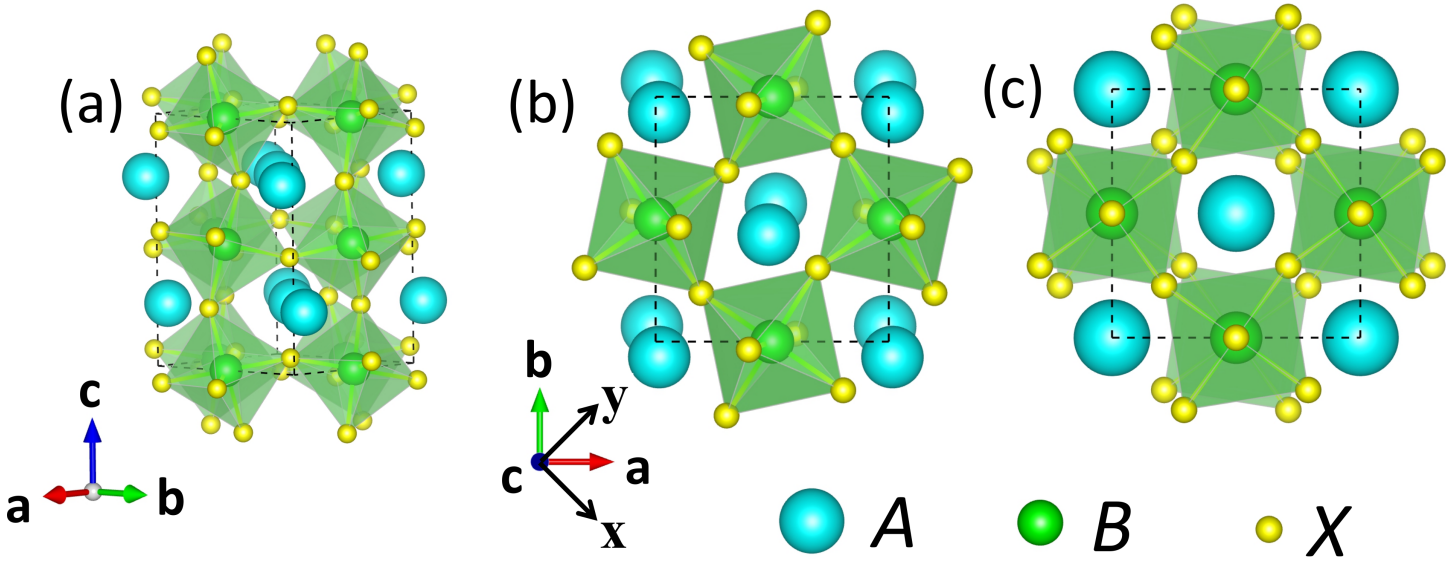

Figure 5: Panels (a) and (b) are sketches of the *Pbnm* perovskite ABX_3. Panel (a) is its three-dimensional view with the anti-phase tilting of BX_6 shown along $\mathbf{a}+\mathbf{b}$ direction; panel (b) is the top view with the in-phase tilting of BX_6 along $\mathbf{c}$ direction (also, z direction). Panel (c) sketches the $I4/mcm$ perovskite ABX_3.

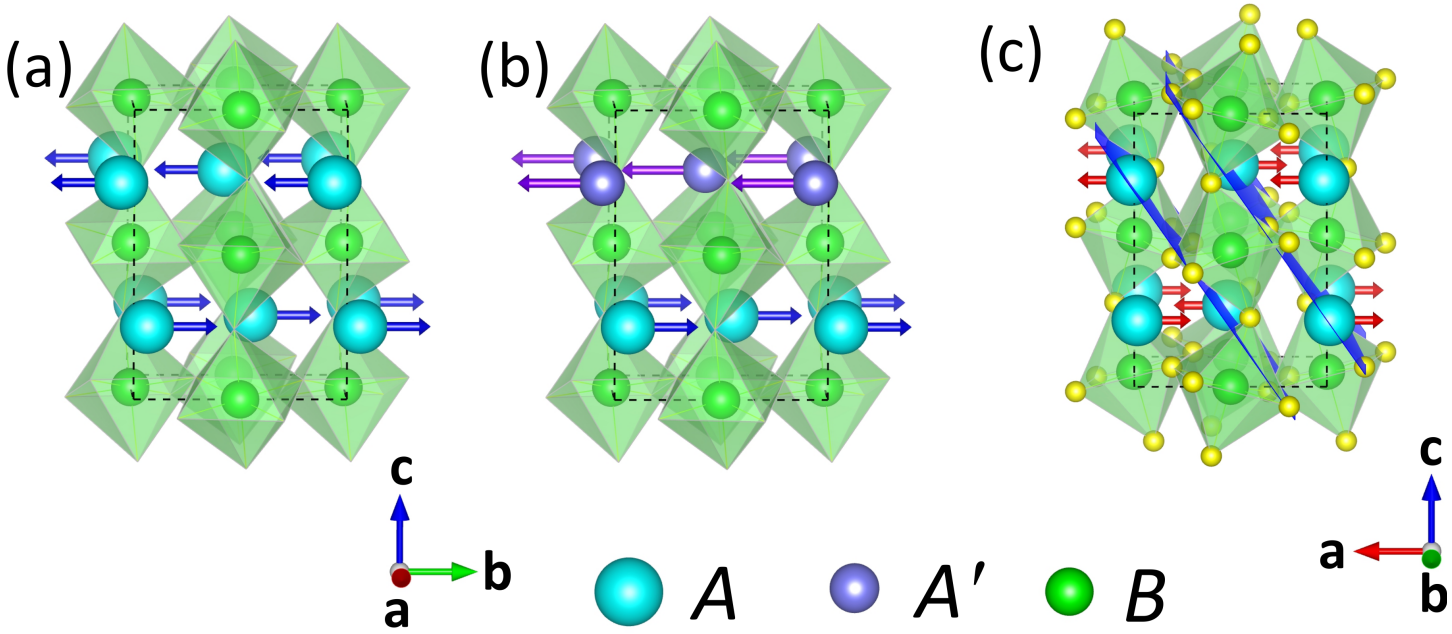

Figure 6: The sketches of the anti-polar motions (of A and A' ions) in perovskites. Panels (a) and (c) are the $(u^{Xz}_{A,x}, -u^{Xz}_{A,y})$, and $(u^{R}_{A,x}, u^{R}_{A,y})$ motions of *Pbnm* ABX_3 perovskite, respectively. Panel (b) shows the displacement mode for $ABX_3/A'BX_3$ superlattice. The lattice and Cartesian coordinate systems coincide with Figure 5.

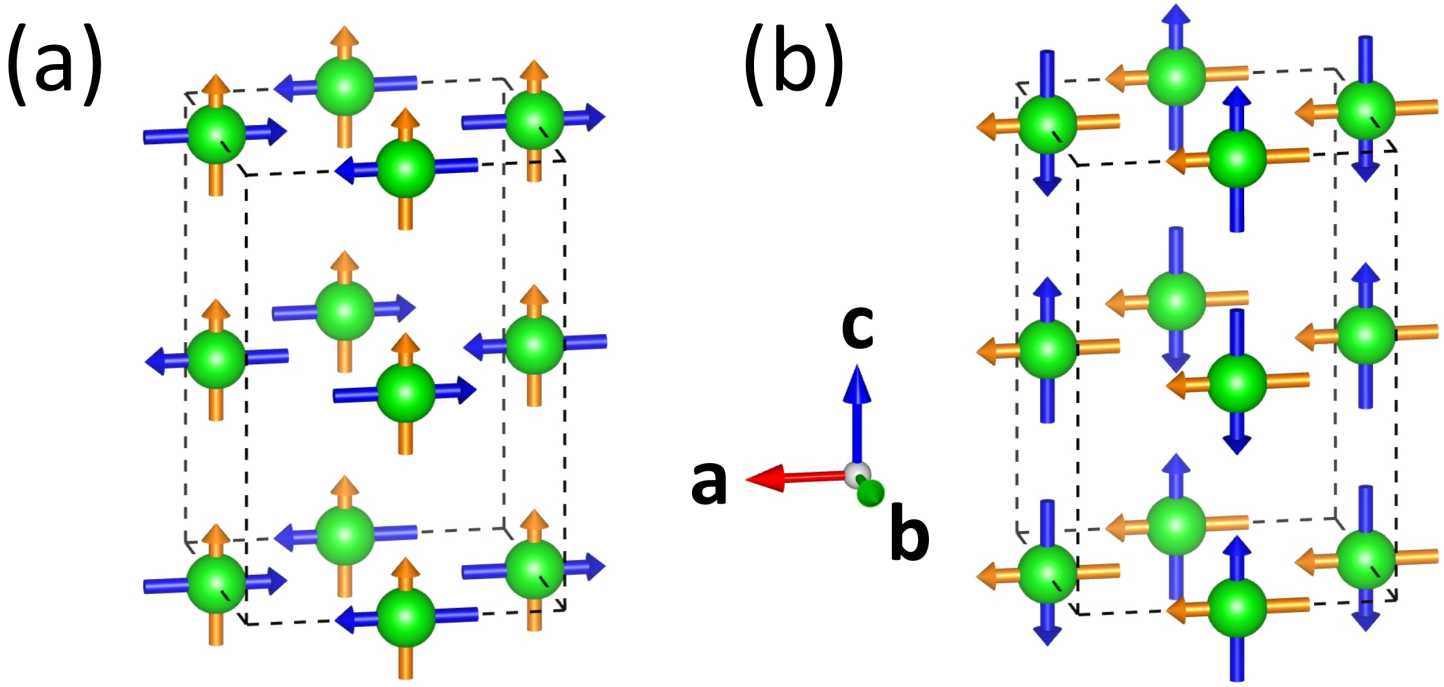

Figure 7: Two typical magnetic structures associated with the $B-$sublattice (green spheres) in ABX_3 perovskites. The blue and yellow arrows denote the $G-$type antiferromagnetic components and weak ferromagnetic components, respectively. The lattice and Cartesian coordinate systems coincide with Figure 5.